The 654-1046 NM line spectrum of the planetary nebula NGC 7027.

J.P. Baluteau, Annie Zavagno, Christophe Morisset, D. Péquignot

Astron. Astrophys. 303, 175–203 (1995)

ASTRONOMY AND ASTROPHYSICS

The 654–1046 nm line spectrum of the planetary nebula NGC 7027*

J.-P. Baluteau[1], **A. Zavagno**[1], **C. Morisset**[2], **and D. Péquignot**[2]

[1] Observatoire de Marseille, URA CNRS 237, 2 Place Le Verrier, F-13248 Marseille Cédex 4, France
[2] Laboratoire d'Astrophysique Extragalactique et de Cosmologie, associé au CNRS (URA 173) et à l'Université Paris 7, DAEC, Observatoire de Paris–Meudon, F-92195 Meudon Principal Cédex, France

Received 21 December 1994 / Accepted 21 February 1995

Abstract. Deep CCD spectra of the planetary nebula NGC 7027, taken over the range 654–1046 nm at a spectral resolution of order 0.1 nm, are presented. About 465 different lines are detected and intensities are provided for 405 features. A total of 680 emission lines is considered.

In the best conditions, namely shortward of 900 nm and outside the telluric absorption bands, emission lines can be detected and measured down to a de-reddened intensity of (1.5–2.5)$\times 10^{-5}$ relative to Hβ. The rate of line detection and identification achieved is a one-order-of-magnitude improvement over previous far-red spectroscopic surveys of nebulae, now superseding available optical surveys. Many of these lines have not been seen before. Altogether, the permitted and forbidden lines encompass 47 ions from 22 elements in this spectral range.

Forbidden lines are produced by 31 ions from 18 elements. Iron-peak elements, notably chromium, manganese, iron, nickel, copper, and possibly vanadium, as well as heavy elements, notably krypton, xenon, selenium, bromine and strontium are detected.

Identification of many permitted lines from high- and low-ionization stages of carbon, nitrogen, and oxygen is reported. Extrapolation of known energy levels is required in some cases. C II, C III, and C IV series discovered in the far red can be followed up to large principal quantum numbers, providing a clue to explain optical lines, left unidentified for tens of years. Available compilations of high-nl atomic energy levels may not be sufficiently comprehensive to fully exploit the nebular spectroscopic data now accessible to common astrophysical devices.

The quadrupolar line [S III]882.98 nm is identified. The natural broadening of the upper autoionizing level of C II 879.4 is disclosed by the peculiar profile of the line. The importance of dielectronic recombination of C II through quartet terms is confirmed by the presence of the strong multiplet C II(14).

The intensity and decrement of the Paschen lines suggest a markedly uneven distribution of dust absorption across the nebula. A diffuse interstellar band and K I lines are detected in absorption.

About 13% of all lines are not identified, a majority of them being weak and affected by large errors. Only 4 of them exceed a de-reddened intensity of $3\times 10^{-4}\, I_\beta$. Some 15 lines are left unidentified, which either exceed a de-reddened intensity of $10^{-4}\, I_\beta$ or are measured with an uncertainty smaller than 20%. Half these unidentified lines are affected by telluric absorption and only 6 fulfill both criteria.

Key words: atomic data – lines: identification – planetary nebulae: NGC 7027 – infrared: ISM: lines

1. Introduction

Kaler et al. (1976) provided a detailed analysis of the spectrum of the planetary nebula NGC 7027 and compiled early far-red measurements, notably by O'Dell (1963) and Schwartz & Peimbert (1973). That reference paper encompassed the spectral range 313–867 nm, combining photographic and spectrophotometric techniques and making use of the thorough line identification performed by Aller et al. (1955, 1963), through the impetus of Bowen. Updates were published by Aller & Keyes (1988) in the spectral range 367–650 nm, using an echelle spectrograph with a CCD detector, and then by Keyes et al. (1990) in the ranges 123.8–320.0 nm (IUE data) and 367.0–875.0 nm.

The first exploration of the far-red region was undertaken just half a century ago by Aller & Minkowski (1946). They used hypersensitized plates and reported about 30 lines longward of Hα. Next to O'Dell and Schwartz & Peimbert, quantitative results were published by Treffers et al. (1976), Scrimger et al. (1978), Condal et al. (1981), and Rudy et al. (1992). These studies however were lacking either sensitivity, spectral resolution, or spectral coverage by optical standards. Keyes et al. (1990) improved on the fluxes of Kaler et al. (1976) shortward of 875.0 nm but mentioned relatively few new spectral features. Thus no systematic line identification of the kind available in

Send offprint requests to: J.-P. Baluteau

* Based on observations made at Observatoire de Haute–Provence
Table 2 is also available in electronic form at CDS via anonymous ftp 130.79.128.5

the optical since 1963 has yet been otained in the far-red for this reference nebula although the CCDs, in current use now, provide good conditions for observing the whole spectrum up to near 1100 nm with high sensitivity, high calibration quality, high dynamical range, and reasonable spectral resolution.

A first discussion of the 681–1045 nm spectrum of NGC 7027, with emphasis on the hydrogen and helium recombination lines, was presented by Péquignot & Baluteau (1988, Paper I). Here we consider again the data used in Paper I and new observational material in a slightly broader wavelength interval with a view to identify the many other lines detected in the far-red. A rewarding aspect of the present work is the discovery of optical and far-red lines from heavy elements (Péquignot & Baluteau 1994, Paper II) and several iron-peak elements.

The observations and data reduction are presented in Sect. 2. Several pieces of the spectrum under study are displayed in Figs. 1–2 of Paper I and Figs. 9–16 of Paper II. Section 3 provides the line intensities and identifications. Figure captions of Paper II are based on these identifications. The results are commented on and compared with previous works in Sect. 4. Some quantitative aspects of the present data, not delt with in Paper I and II, will be discussed in Paper IV (Péquignot et al., in preparation).

2. Observations and data reduction

2.1. Spectrophotometric data

Observations of NGC 7027 were carried out from 1986 to 1988, using the CARELEC spectrograph (Lemaitre et al. 1990) attached to the Cassegrain focus of the 1.93 m telescope at the Observatoire de Haute–Provence (France). Two RCA CCDs (320 × 512 array of 30μm individual pixels) and one Thomson CCD (383 × 576 array of 25μm individual pixels) were used as detectors to cover quite homogeneously and uniformly all the visible and far-red spectrum with a read-out noise of about 120, 65 and 12 electrons for RCA#1, RCA#3, and Thomson respectively. As a result of a compromise between a large spectral domain and the ability to separate as much as possible all spectral features of the nebula, a grating dispersion of 3.3 nm/mm has been selected. The spectra were aligned along the columns of the detector array.

With a scale of 1.20 arcsec per pixel, a slit width of 3 arcsec was chosen, somewhat larger than normal seeing conditions. In all observations of NGC 7027 reported here, the 5 arcmn spectrograph slit was oriented in a North-South direction, passing through the brightest optical condensation. An implication of this spatial configuration is discussed in Sect. 4.4.2.

Table 1 summarizes the observing runs. Spectra secured shorward of Hα will be presented in Paper V (Baluteau et al., in preparation; see also Paper II, notably Figs. 1–8). At long wavelengths the quantum efficiency of the CCD drops rapidly and only data shortward of 1046 nm are discussed here.

Table 1. Log of observations

Code	$\Delta\lambda$(nm)	Exp. time (min)	Date	Atm.[a]	Stars[b]
N29B	632–681	0.13,0.5,2,8,30,120	87/09/18	A	1
N22	662–711	3,120	87/06/26	B	2
N13A	681–731	20,90	86/11/24	A	1
N28B	710–759	0.5,2,8,30,120	87/09/17	B	1
N06B	730–780	5,15,45	86/06/04	C	2
N12A	747–796	120	86/11/23	C	1
N28A	774–822	20,120	87/09/17	A	1, 2
N11A	794–843	120	86/11/22	C	1
N23B	802–850	60	87/06/27	B	2
N24B	802–850	120	87/06/28	A	2
N03	840–889	60	86/06/01	A	2
N26B	858–906	120	87/09/15	A	1
N14A	884–932	90	86/11/25	A	1
N27B	905–950	0.5,2,8,30,120	87/09/16	A	1
N14B	930–977	80	86/11/25	A	1
N01	966–1012	60	86/05/31	C	2
N15A	1001–1046	120	86/11/26	C	3
N36	633–977	1,2,4,8,16,32	88/08/13	A	1, 2

[a] Atmospheric conditions: A = good, B = mean, C = poor.
[b] Standard stars: 1 = HD19445, 2 = BD+26.2606, 3 = α Lyr.

2.2. Data reduction

2.2.1. Flat–fielding procedure

An internal continuum source is used to correct for wide and short range, pixel to pixel, variations in quantum efficiency due to local changes or fringing effects. The efficiency of the procedure to provide a normalized spectrum has been checked for each spectral range by comparing spectra of a standard star measured on different locations (columns) over the CCD. R.m.s. noise values typically less than 1% are obtained for wavelengths shorter than about 900 nm. At longer wavelengths, because of increased fringe contrast (Thomson CCD excepted), higher systematic errors are measured (up to 20% around 1050 nm).

2.2.2. Spike removal

The CCD columns effectively used to observe the objects are chosen so as to be virtually free from "hot" pixels. Because of the long exposure time required for the observations (up to two hours) the number of spikes in the CCD picture is quite significant. An automated procedure is used to clean the raw picture. The procedure is based on the fact that the line spatial profile, along the spectrometer slit, is quite similar to the continuum profile. An averaged spatial profile is calculated, over neighbouring CCD rows, and subsequently subtracted, after normalization, from the running individual row. The pixel which yields the highest deviation, if greater than the nominal noise figure, is corrected using the averaged value. Normally two iterations of the cleaning procedure are sufficient to provide the correct final CCD picture.

Table 2. Lines in the spectrum of NGC 7027. *Comments:* (a) in the wing of a nearby strong line, (b) difficult continuum level estimate, (c) blend with nearby lines, (d) broad feature.

Identification	λ_{theo}	λ_{obs}	n	$10^4 F/I_\beta$	Error (%)	Comments
[N II](1F)	654.81	654.80	3	8310.0	3	
He II(6)	656.02	656.01	1	2460.0	8	
Hα	656.28	656.29	4	73700.0	3	
C II(2)	657.80	657.78	1	60.0	50	(a)
{C II(2)	658.28}					
{[N II](1F)	658.34}	658.32	4	24700.0	3	
{O V(7.01)	660.13}					
{[Fe VII](1F)	660.14}	660.10	1	1.7	45	(a)
X		661.06	1	1.4	60	(a)
X abs		661.31	1	–	–	in absorption
X		661.75	1	1.6	50	(a)
O II(4)	662.74	662.70	2	0.6	60	(c)
[Cs V](1F)	663.06	663.00	2	0.7	50	(c)
O II(4)	664.11	664.13	2	0.5	75	
X		665.51	2	2.2	30	(d)
{O II(4)	666.67}					
{[Ni II](2F)	666.68}	666.62	2	0.9	40	(c)
X		666.85	2	1.2	30	(c) C II(5g-13h)
X		667.20	2	1.8	40	(a), (d)
He I(46)	667.82	667.82	8	766.0	2	
He II(5-13)	668.32	668.36	7	105.0	3	
{[I III](1F)	670.87}					
{[Mn II](2F)	670.91}					
{[Cr V](2F)	670.97}	670.95	3	2.5	25	(a)
[S II](1F)	671.65	671.63	8	503.0	3	
O II(4)	672.14	672.17	3	1.8	50	(b)
{C III(3)	672.74}					
{[S II](1F)	673.08}	673.07	8	1160.0	2	
{C III(3)	673.10}					
{[Cr IV](2F)	673.40}					
{[Fe IV](^{4}G-^{2}I)	673.44}	673.50	2	2.0	50	(a)
{[Sr II](1F)	673.84}					
{[Fe IV](^{4}G-^{2}I)	673.98}	673.95	3	4.2	6	
{C III(3)	674.22}					
{He I\1/21	674.41}					
{C III(3)	674.44}	674.44	3	6.0	5	(c)
{C IV(9-16)	674.69}	674.69	3	4.4	6	(c)
{N V(9-12)	674.70}					
{[Cr IV](2F)	674.76}					
{He I\1/20	675.58}	675.57	3	1.1	40	
{[Fe IV](^{4}P-^{2}D)	675.60}					
{[Fe IV](^{4}P-^{2}D)	676.14}	676.17	3	2.1	15	(d)
{C III(3)	676.22}					

Table 2. (continued)

Identification	λ_{theo}	λ_{obs}	n	$10^4 F/I_\beta$	Error (%)	Comments
[Mn II](2F)	676.35	676.33	2	0.5	80	(c)
{[Xe IV](2F)	676.89}					
{He I\1/19	676.95}	676.98	2	0.6	70	
{C IV(10-25)	677.87}					
{C II(14)	677.99}	678.00	5	11.8	3	
{C II(14)	678.06}					
C II(14)	678.39	678.42	3	2.1	15	(c)
{He I\1/18	678.57}					
{C II(14)	678.72}	678.70	3	3.7	7	(c)
{C II(14)	679.15}	679.14	3	4.9	10	(c)
{[Fe IV](^{4}P-^{2}D)	679.25}					
[K IV](1F)	679.50	679.50	3	29.2	3	
{C II(14)	679.80}	679.80	2	0.7	60	(c)
{[Kr IV](2F)	679.85}					
C II(14)	680.07	680.07	3	2.8	15	
He I\1/17	680.48	680.48	2	0.6	70	(b)
C II(14)	681.23	681.15	1	0.5	80	(b)
{Si II(7.20)	681.85}					
{[Fe V](^{3}P-^{1}S)	681.92}	682.06	1	1.5	50	(d)
{X	}					C II(5f-12g)
{[Kr III](1F)	682.69}	682.66	2	15.9	5	
{He I\1/16	682.79}					
{C I(21)	682.81}					
Si II(7.20)	682.98	682.99	2	2.1	20	(a)
X		683.26	2	1.2	40	(d)
O II(45)	684.68	684.70	1	0.6	80	
{[Mn II](2F)	685.04}					
{[Mn VI](1F)	685.21}	684.96	3	9.2	4	
{He I\1/15	685.59}	685.60	2	1.5	30	
{C III(19)	685.73}					
{[Sr II](1F)	686.82}					
{X	}	686.94	1	1.5	50	atm.40%
C III(19)	687.17	687.20	1	1.2	60	atm.34%
{[Fe II](43F)	687.38}	687.41	2	2.9	40	(b), (d)
{C IV(7p-9d)	687.46}					C II(5g-12h)
{C IV(7p-9d)	687.58}					atm.28%
X		688.09	2	1.2	50	C II(5d-11f), atm.28%
{He I\1/14	689.05}					
{He II(5-12)	689.09}	689.06	4	177.0	4	atm.18%
O II(45)	689.51	689.52	2	4.7	15	(a) atm.10%
{[Fe II](14F)	689.62}					
{[Cr IV](2F)	689.65}	689.70	1	2.3	25	(a) atm.22%
X		690.11	2	1.8	30	atm.16%
O II(45)	690.64	690.61	2	3.6	14	atm.13%

Table 2. (continued)

Identification	λ_{theo}	λ_{obs}	n	$10^4 F/I_\beta$	Error (%)	Comments
{O II(45)	690.79}					
{O II(45)	691.06}	691.02	2	2.5	15	atm.12%
[Cr IV](2F)	691.48	691.42	2	1.8	35	atm.9%
He I\1/13	693.39	693.36	2	2.1	20	atm.12%
[Cu IV](^{3}F-^{1}D)	694.90	694.89	2	2.5	20	C III(7g-13h)?, atm.10%
{N III(3p''^{2}D-4d'^{2}F°)	695.73}					
{X	}	695.87	2	4.0	10	(d) atm.10%
{[Co III](^{4}F-^{4}P)	696.14}					
{X	}	697.60	2	1.8	30	C III(7h-13i)?
{[Mn II](2F)	697.85}					
X		698.24	2	0.9	50	C III(7i-13k)?
He I\1/12	698.94	698.94	2	4.0	30	(d) C III(7f-13g)?, atm.7%
{X						
{[Fe IV](^{4}P-^{2}D)	699.71}	699.74	2	3.1	10	(d) atm.6%
{[Xe V](1F)	699.85}					
O I(21)	700.21	700.20	2	12.0	50	(a)
[Ar V](1F)	700.57	700.57	4	1100.0	4	atm.8%
X		701.10	2	2.3	50	(a), (d)
C IV(10-23)	702.14	702.19	2	1.2	50	
X		702.90	1	1.4	50	(c) atm.7%
O IV(12.01)	703.23	703.22	2	4.0	8	O IV(7g-9h)?
{[Fe IV](^{4}P-^{2}D)	703.63}					
{C III(6.01)	703.72}	703.72	2	1.6	25	(d)
{N V(11-18)	703.78}					
X		704.70	2	1.6	30	N IV(7h-9i)?
{[Cr IV](2F)	705.17}					O IV(7h-9i)?
{O IV(12.01)	705.36}	705.38	2	4.9	40	(b), (d)
{He I\1/11	706.22}					N IV(7i-9k)?
{C IV(7-9)	706.24}					O IV(7i-9k)?
{He I(10)	706.53}	706.54	4	2100.0	3	
{C I(26.01)	707.49}					
{C I(26.01)	707.65}	707.66	2	1.2	40	(b)
C I(26.01)	708.78	708.89	2	1.0	50	(b)
[Pb II](^{2}P-^{2}P)	709.98	710.02	2	1.4	40	(c)
X		710.32	2	1.4	40	(c) C II(5f-11g)
{[Cr IV](2F)	711.09}					
{C I(26)	711.15}					
{C II(20)	711.25}					
{C II(20)	711.30}	711.27	2	4.7	50	(b), (d)
{C I(26)	711.32}					
{Si II(7.19)	711.34}					
{C I(25.02)	711.52}					
{C I(26)	711.52}	711.58	2	3.7	50	(b)
{C II(20)	711.56}					

Table 2. (continued)

Identification	λ_{theo}	λ_{obs}	n	$10^4 F/I_\beta$	Error (%)	Comments
{C I(25.02)	711.70}					
{C I(25.02)	711.97}					
{C II(20)	711.99}	712.00	1	4.1	40	(d)
{C II(20)	712.57}					
{Si II(7.19)	712.58}	712.61	1	4.1	25	(a)
[Ar III](1F)	713.58	713.55	5	7430.0	3	
[Co III](^{4}F-^{4}P)	715.26	715.17	3	2.0	60	(b)
[Fe II](14F)	715.52	715.50	4	29.6	9	(b)
He I\1/10	716.05	716.06	3	9.1	25	(b) C II(5g-11h)
{[Ar IV](2F)	717.05}	717.06	4	185.0	3	atm.17%
{[Fe II](14F)	717.20}					
He II(5-11)	717.75	717.76	4	230.0	8	atm.28%
[Fe IV](^{4}D-^{4}F)	718.40	718.48	1	2.1	60	atm.19%
[Fe IV](^{4}D-^{4}F)	719.16*	719.06	2	3.7	50	atm.21%, (* 3 lines)
C IV(9-15)	720.66	720.66	3	4.2	35	atm.18%
{C III(39)	721.05}					
{C III(39)	721.23}	721.22	3	3.5	50	(d) atm.3%
{C IV(8s-11p)	721.35}					
{[Cs III](^{2}P-^{2}P)	721.97}	722.11	2	4.1	40	(d) atm.7%
{[Fe IV](^{4}D-^{4}F)	722.28}					
C II(3)	723.11	723.12	4	39.4	6	atm.10%
{C II(3)	723.62}					
{[Ar IV](2F)	723.75}	723.72	4	229.0	4	atm.14%
{OI(20)	725.44}	725.44	4	11.7	25	atm.24%
{[Ni II](2F)	725.58}					
[Ar IV](2F)	726.2 7	726.28	4	153.0	6	atm.13%
X		726.68	2	4.7	50	(a) C II(5d-10f), atm.18%
He I(5)	728.13	728.12	3	283.0	4	atm.14%
[Ca II](1F)	729.15	729.10	1	1.5	50	atm.11%
He I\1/9	729.79	729.80	2	8.3	20	atm.3%
{O III(24.03)	730.70}	730.67	2	4.8	25	(a) atm.3%
{[Ni II](2F)	730.77}					
{[O II](2F)	731.99}					
{[O II](2F)	732.00}	732.01	4	6520.0	2	atm.6%
{[O II](2F)	732.96}					
{[O II](2F)	733.02}	733.01	4	5160.0	4	atm.3%
{[Ar IV](2F)	733.15}					
X		734.52	2	2.2	30	atm.5%
X		735.42	2	2.0	30	atm.5%
{C IV(10-21)	736.39}					
{O III(24.03)	736.52}	736.53	2	1.3	30	(d) atm.5%
{[Br IV]	736.80}					
{C II(3p'^{2}D-3d'^{2}P^o)	737.00}	737.01	2	2.3	20	atm.6%

Table 2. (continued)

Identification	λ_{theo}	λ_{obs}	n	$10^4 F/I_\beta$	Error (%)	Comments
{[Ni II](2F) {[Zr VII]($^3_2$P-^{3}P$_1$)	737.78} 737.87}	737.77	3	12.4	3	atm.3%
{C IV(6p-7d) {C IV(6p-7d)	738.03} 738.24}	738.10	2	0.9	50	atm.4%
[Br III](2F)	738.51	738.43	2	1.0	50	atm.5%
[Fe II](14F)	738.82	738.80	3	5.4	5	
[Cr IV](1F)	739.13	739.17	2	1.2	50	
{[Ni II](2F) {O III (24.03)	741.16} 741.40}	741.28	2	2.1	15	(d)
X		741.80	2	2.7	30	(d)
N I(3)	742.36	742.36	2	1.0	50	
N V(10-14)	744.02	744.00	2	1.8	40	(c), (d)
N I(3)	744.23	744.29	2	1.9	35	(c)
[Fe II](14F)	745.25	745.22	3	10.2	13	
O III(24.03)	745.53	745.55	2	2.3	15	
{C II(17.10) {Si III(8.03)	746.18} 746.23}	746.25	2	1.9	30	(d)
N I(3)	746.83	746.85	2	2.7	25	
X		747.35	2	2.7	25	C III(7g-12h)?
C III(41)	748.65	748.70	3	3.4	20	atm.4%
He I\1/8	749.97	749.98	4	12.8	15	atm.3%
C II(17.13)	750.53	750.48	2	1.2	50	(c)
X		750.76	3	2.3	25	(c) C III(7h-12i)?
X		751.05	2	2.0	30	(c) C II(5f-10g)
O III(24.03)	751.60	751.52	3	3.0	30	(d) C III(7i-12k)?
C II(17.13)	751.99	751.99	2	1.5	40	
[Cl IV](1F)	753.00	753.04	5	205.0	3	C III(7f-12g)?
[Xe IV](1F)	753.54	753.50	3	7.4	4	
X		757.41	2	1.9	30	C II(5g-10h)
C III(35)	757.82	757.83	2	6.2	15	(d)
{[Cr V](1F) {N IV(6g^1-7h^1) {N IV(22)	758.06} 758.15} 758.24}	758.18	2	5.7	10	(d)
{[Mg I](1F) {N V(11-17)	758.47} 758.54}	758.48	2	0.9	50	
{O V(29) {C III(35) {He II(5-10)	759.20} 759.23} 759.27}	759.33	2	385.0	12	atm.23%
{O V(30) {C III(35)	761.09} 761.26}	761.10	1	10.5	30	atm.67%
N V(13)	761.85	761.83	1	7.6	12	atm.12%
[Fe II](1F)	763.75	763.66	1	6.2	25	atm.41%
K I(1) abs	766.49	766.42	2	–		in absorption, atm.22%

Table 2. (continued)

Identification	λ_{theo}	λ_{obs}	n	$10^4 F/I_\beta$	Error (%)	Comments
O IV(20)	767.74	767.63	2	13.5	8	atm.12%
{N III(24)	768.68}	768.67	2	4.1	20	
{[Fe II](1F)	768.69}					
K I(1) abs	769.90	769.83	2	–		in absorption
N IV(23)	770.30	770.34	2	10.8	8	
{C IV(6d-7f)	770.67}	770.69	2	2.6	30	
{C III(10.01)	770.74}					
O IV(21)	771.33	771.29	2	31.0	6	
{Si IV(19)	771.88}					
{X	}	771.95	2	3.9	20	Ne IV(6g-7h)??
X		772.25	2	2.7	50	(a) N IV(8h-11i)?
{Si IV(22)	772.38}					
{[S I](3F)	772.50}					O IV(8h-11i)?
{C IV(8.01)	772.62}	772.64	2	119.0	5	N IV(8i-11k)?
X		773.15	2	1.2	60	(c) O IV(8i-11k)?
[Fe II](1F)	773.32	773.30	2	2.6	40	(c) N IV(8k-11l)?
{C IV(8-11)	773.60}	773.57	2	14.0	5	O IV(8k-11l)?
{O VI(8-9)	773.65}					
[V IV](2F)	774.15	774.01	2	1.3	60	
X		774.65	1	4.8	50	(a) Ne IV(6h-7i)??
[Ar III](1F)	775.11	775.12	4	2160.0	3	
{O I(1)	777.20}					
{O I(1)	777.42}	777.38	2	4.9	14	(d)
{O I(1)	777.54}					
X		780.90	2	0.9	50	
He I\2/13	781.16	781.18	2	0.9	50	
He I\1/7	781.60	781.63	2	21.2	4	
O III(26.06)	782.07	782.12	2	0.6	70	
O III(26.06)	783.25	783.30	2	0.6	70	
O III(26.06)	783.93	783.90	2	1.5	30	
O III(26.03)	784.80	784.83	2	0.8	50	
X		785.49	2	0.9	40	
[V IV](2F)	785.73	785.73	2	1.4	40	(c)
C IV(9-14)	786.08	786.09	2	9.0	15	C II(5d-9f)
{O III(26.03)	787.37}					
{[P II](3F)	787.60}	787.61	3	46.4	3	atm.5%
{Mg II(8)	787.70}					
He I\2/12	788.08	788.08	2	1.4	30	(a)
[Cr V](1F)	788.44	788.36	2	5.8	10	(c)
X		788.67	2	1.4	40	(c)
[Ni III](^{3}F-^{1}D)	788.99	788.98	2	3.1	20	atm.3%
He I\4/37	789.29	789.25	2	0.6	80	(c)

Table 2. (continued)

Identification	λ_{theo}	λ_{obs}	n	$10^4 F/I_\beta$	Error (%)	Comments
{He I\4/36	789.57}					
{Mg II(8)	789.64}	789.63	2	4.2	18	atm.8%
He I\4/35	789.87	789.90	2	0.7	60	(c)
He I\4/34	790.21	790.30	2	0.5	90	(c)
He I\4/33	790.58	790.60	2	0.6	80	(c)
{He I\4/32	790.98}					
{X	}	791.30	2	3.0	20	(d)
{He I\4/31	791.41}					C III($6d^3$-$8f^3$)??
He I\4/30	791.90	791.96	2	0.8	50	atm.4%
{He I\4/29	792.44}					
{[Fe IV](^{4}D-^{2}F)	792.50}	792.55	2	1.4	30	(d) atm.4%
{He I\4/28	793.03}	793.08	2	0.8	50	
{[Te III](1F)	793.33}					
He I\4/27	793.70	793.71	2	1.3	40	
He I\4/26	794.44	794.48	2	1.2	50	(c)
{O I(35)	794.75}					
{C IV(6d-7p)	794.81}	794.83	2	2.9	25	(c) atm.3%
{O I(35)	795.08}					
{O I(35)	795.22}	795.13	2	2.7	20	(c), (d)
{He I\4/25	795.28}					
{[Zr VII](^{3}P$_2$-^{3}P$_0$)	796.14}					
{He I\4/24	796.23}	796.30	2	2.3	20	(c) atm.6%
{O III(26.03)	796.35}					
{He I\2/11	797.15}	797.21	2	1.9	30	(d)
{He I\4/23	797.30}					
He I\4/22	798.53	798.57	2	1.6	35	
X		799.25	2	1.4	40	
{[As II](2F)	799.78}					
{He I\4/21	799.94}	799.95	2	2.8	25	
{[Cr II](1F)	800.01}					
{C I(31)	801.50}					
{He I\4/20	801.58}	801.57	2	2.0	30	(c)
{C I(31)	801.86}					
{N III(26)	801.91}	801.90	2	2.5	20	(c)
{C III(44)	802.11}					
{C I(31)	802.13}	802.15	2	1.2	40	(c)
{[Y V](^{2}P-^{2}P)	802.36}					
{X	}	802.55	4	2.6	50	(d)
He I\4/19	803.48	803.50	4	2.3	20	atm.4%
X		804.02	2	1.9	45	(c), (d)
[Cl IV](1F)	804.56	804.55	5	561.0	3	atm.4%
{[Te II](1F)	804.96}					
{O III(50)	805.15}	805.10	4	2.0	30	
He I\4/18	805.73	805.78	4	3.2	20	(c)
O III(5fG-6gH)	806.01	806.00	4	1.3	30	(c)

Table 2. (continued)

Identification	λ_{theo}	λ_{obs}	n	$10^4 F/I_\beta$	Error (%)	Comments
O III(50)	806.25	806.24	4	1.8	25	(c) atm.3%
{He II(6-34)	846.37}					
{P17	846.73}	846.73	3	255.0	3	atm.5%
{He II(6-33)	848.05}					
{He I\3/11	848.06}					
{[Cl III](3F)	848.09}	848.08	3	39.2	4	
{He I\6/16	848.62}	848.62	3	9.1	17	
{He I\7/16	848.86}					
{He I\5/16	848.88}					
X		849.50	3	3.7	25	atm.4%
{Ca II(2)	849.80}					
{He II(6-32)	849.89}					
{[Cl III](3F)	850.00}					
{P16	850.25}	850.27	3	328.0	3	atm.8%
{He I\2/8	851.79}					
{He II(6-31)	851.93}	851.95	1	12.3	8	
{He I\10/17	852.88}					
{He I\6/15	852.89}	852.90	1	12.5	8	
{He I\7/15	853.14}					
{He I\5/15	853.21}					
{He I\9/17	853.34}					
[I III](1F)	853.65	853.62	1	1.4	60	
{He II(6-30)	854.18}					
{Ca II(2)	854.21}					
{P15	854.54}	854.56	1	358.0	3	
{[Cl III](3F)	854.80}					
{He I\10/16	856.46}					
{He II(6-29)	856.69}	856.73	1	15.2	7	
{He I\9/16	857.01}					
{[Fe V](^{3}H-^{1}G)	857.85}					
{[Cl II](1F)	857.87}	857.90	1	209.0	3	
{He I\6/14	858.17}					
{He I\4/10	858.25}					
{He I\7/14	858.43}					
{He I\5/14	858.58}					
{He II(6-28)	859.48}					
{P14	859.84}	859.85	2	432.0	3	
X		860.50	2	2.0	40	(a) C III($6f^1$-$8g^1$)?
He I\10/15	860.82	860.84	2	2.2	30	
{He I\9/15	861.49}					
{[V III](2F)	861.59}					
{[Fe II](13F)	861.69}	861.66	2	36.0	3	
O III(50)	807.02	807.00	4	1.9	30	
O III(5fG-6gH)	807.68	807.61	4	1.6	25	
{He I\4/17	808.42}	808.42	4	4.2	25	
{O III(50)	808.42}					

Table 2. (continued)

Identification	λ_{theo}	λ_{obs}	n	$10^4 F/I_\beta$	Error (%)	Comments
He I\2/10	809.40	809.40	4	1.5	50	
{Si III(37)	810.28}	810.32	4	1.6	40	
{Si III(37)	810.35}					
He I\4/16	811.63	811.63	4	2.5	25	
{[Cr II](1F)	812.53}					
{O III(5fG-6gH)	812.75}	812.67	1	1.3	60	atm.20%
[Fe V](^{3}H-^{1}I)	813.72	813.63	4	2.6	30	atm.14%
{X	}	814.01	4	2.6	30	C II(5f-9g)
{[Br III](2F)	814.24}					atm.16%
O III(5fD-6gF)	814.57	814.65	1	1.6	60	atm.20%
O III(5fD-6gF)	815.23	815.25	1	1.6	60	atm.20%
He I\4/15	815.57	815.60	4	3.1	50	atm.19%
{N IV(6p^1-7s^1)	815.96}					
{X	}	816.02	4	6.8	20	atm.30%
O III(5fG-6gH)	816.80	816.84	4	2.5	30	atm.28%
X		817.75	4	2.6	30	atm.38%
{N I(2)	818.49}					
{N I(2)	818.80}	818.70	4	6.0	15	(d) atm.18%
{C III(5g'^{3}H°-6h'^{3}I)	818.91?}					C III 818.6 assumed
C III(43)	819.65	819.67	5	161.0	20	atm.19%
N I(2)	820.04	820.00	2	2.3	70	(a) atm.19%
He I\4/14	820.39	820.40	4	5.3	20	
{[Cs VI](^{3}P$_2$-^{3}P$_0$)	821.06}					
{N I(2)	821.07}	821.05	2	2.9	50	(a) atm.19%
N I(2)	821.63	821.56	4	8.8	25	(b), (d) C II(5g-9h)
						atm.4% C II(5p-7d)?
{N I(2)	822.31}	822.27	3	5.5	40	(b), (d) C II(5p-7d)?
{C III(5f'^{3}G-6g'^{3}H^0)	822.62?}					C III 822.3 assumed, atm.14%
{O III(5gH-6hI)	822.76}	822.78	3	5.1	40	(b) atm.50%
{[Cr II](1F)	822.97}					
{He II(5-9)	823.68}	823.67	3	638.0	6	atm.10%
{O III(5gG-6hH)	823.85}					
{N I(2)	824.24}					
{[Kr V](1F)	824.31}	824.27	3	13.0	35	(b), (c) atm.22%
O III(5gG-6hH)	824.41	824.46	2	4.7	60	(b), (c) atm.22%
{P40	824.99}					Change of
{O III(5gF-6hG)	825.08}	825.10		59.6	10	continuum for
{P39	825.24}					$\lambda > 825$ nm
{P38	825.50}					
{P37	825.78}	825.65		66.0	10	
P36	826.09	826.11	3	55.6	8	C III(6g-8h)?, atm.7%
{P35	826.43}	826.45	3	64.3	7	atm.8%
{He I\4/13	826.44}					
{P34	826.79}	826.79	3	52.1	6	
{O III(5gH-6hI)	826.88}					

Table 2. (continued)

Identification	λ_{theo}	λ_{obs}	n	$10^4 F/I_\beta$	Error (%)	Comments
P33	827.19	827.20	3	45.2	8	atm.15%
P32	827.63	827.63	3	48.6	9	atm.21%
P31	828.11	828.12	3	56.3	12	C III(7g-11h)?, atm.21%
{P30	828.64}	828.65	3	64.9	8	atm.13%
{O III(5gF-6hG)	828.67}					
P29	829.23	829.23	3	64.3	4	atm.6%
P28	829.88	829.88	3	72.5	6	atm.8%
P27	830.61	830.61	3	79.6	6	atm.15%
{P26	831.43}	831.39	3	106.0	6	(d) C III(6h-8i)?
{C III(5g'^{3}F^o-6h'^{3}G)	831.51?}					C III 831.2 ass., atm.8%
{He II(6-50)	831.99}					
{P25	832.34}	832.34	3	106.0	5	C III(7h-11i)?
{He II(6-49)	832.50}					
						atm.4%
{He II(6-48)	833.02}					
{C III(12.01)	833.30}					C III(7i-11k)?
{P24	833.38}	833.38	3	118.0	5	atm.11%
{He II(6-47)	833.60}					
{C III(12.01)	834.16}					
{He II(6-46)	834.21}					
{He I\4/12	834.22}					
{[Fe V](^{3}H-^{1}I)	834.27}					
{P23	834.56}	834.55	3	138.0	8	
{C III(12.01)	834.79}					
{He II(6-45)	834.86}					
X		835.27	3	4.3	30	(b) atm.8%
{He II(6-44)	835.55}					
{C III(12.01)	835.79}					
{C III(12.01)	835.87}					
{P22	835.90}	835.89	3	173.0	4	atm.4%
{He I\1/6	836.16}					
{He II(6-43)	836.30}					
{He I\3/12	836.93}					
{He II(6-42)	837.10}					
{P21	837.45}	837.44	3	142.0	4	atm.6%
{He I\6/20	837.64}					
{He I\5/20	837.77}					
{He I\7/20	837.88}					
{He II(6-41)	837.96}	838.00	3	6.3	15	
X		838.72	3	17.3	15	atm.4%
{He II(6-40)	838.89}					
{P20	839.24}	839.25	3	162.0	8	
{He I\6/19	839.73}					
{He I\5/19	839.88}					
{He II(6-39)	839.89}	839.89	3	9.9	30	(b)
{He I\7/19	839.97}					
X		840.58	3	6.6	13	C III($6f^3$-$8g^3$)

Table 2. (continued)

Identification	λ_{theo}	λ_{obs}	n	$10^4 F/I_\beta$	Error (%)	Comments
{He II(6-38)	840.98}					
{P19	841.33}	841.33	4	190.0	3	atm.5%
{He II(6-37)	842.16}					
{He I\6/18	842.18}	842.19	4	15.4	17	
{He I\5/18	842.37}					
{He I\7/18	842.43}					
X		842.93	2	3.5	35	(a) atm.3%
{[Cl III](3F)	843.36}	843.37	3	41.8	10	(a) atm.4%
{He II(6-36)	843.44}					
P18	843.80	843.80	3	215.0	3	atm.6%
{He I\4/11	844.44}					
{O I(4)	844.64}	844.65	3	168.0	8	atm.8%
{He II(6-35)	844.84}					
{He I\6/17	845.10}	845.24	3	12.5	25	(a)
{He I\5/17	845.32}					
{He I\7/17	845.35}					
{[V III](2F)	845.73}					
{X	}	845.92	3	3.0	15	atm.4%
He II(6-27)	862.61	862.63	2	18.1	5	
X		862.90	2	2.3	30	
{He I\3/10	863.26}					
{X	}	863.35	2	6.3	15	
{He I\6/13	864.81}	864.84	2	22.2	4	
{He I\7/13	865.07}					O IV(3p'''-5p')?
{C III(40)	865.26}					
{He I\5/13	865.33}					
{He II(6-26)	866.14}					
{He I\10/14	866.20}					
{Ca II(2)	866.21}					
{C III(45)	866.36}					
{P13	866.50}	866.50	2	591.0	3	
{C III(45)	866.52}					
{He I\9/14	867.04}					
{N I(1)	868.03}					
{[V III](1F)	868.28}					
{N I(1)	868.34}	868.30	2	11.5	15	(d)
{N I(1)	868.61}					
{He II(6-25)	870.13}	870.15	2	23.3	3	
{N I(1)	870.32}					
{C IV(10-17)	870.66}					
{X	}	870.70	2	6.1	13	
N I(1)	871.17	871.15	2	4.3	35	(b)
N I(1)	871.88	871.94	2	2.7	40	(b)
{[C I](3F)	872.72}	872.72	2	138.0	6	
{He I\10/13	872.97}					

Table 2. (continued)

Identification	λ_{theo}	λ_{obs}	n	$10^4 F/I_\beta$	Error (%)	Comments
{He I\6/12	873.33}	873.36	2	23.0	5	
{He I\7/12	873.59}					
{He I\5/12	873.99}	874.06	2	2.6	50	(b)
{He I\9/13	874.04}					
{He II(6-24)	874.68}					
{P12	875.05}	875.05	2	702.0	4	
X		876.11	2	1.1	60	(a)
X		876.73	2	1.4	50	(d)
He I\4/9	877.66	877.68	2	20.7	4	
[P I](1F)	878.76	878.80	2	1.1	60	(c)
X		879.13	2	1.5	50	(c)
C II(28.01)	879.38	879.44	2	11.8	5	(d)
{He II(6-23)	879.89}	879.89	2	35.3	4	
{C II(28.01)	879.99}					
{[Fe V](^{3}H-^{1}G)	880.01}					
Mg I(7)	880.68	880.67	2	5.3	15	
He I\10/12	881.65	881.66	2	3.3	20	
{O IV(3p'''^{2}P^o-5p'^{2}D)	882.90}					
{[S III](1F)	882.97}	882.98	2	9.8	15	(d)
{He I\9/12	883.04}					
{He I\6/11	884.52}	884.54	2	38.7	4	
{He I\7/11	884.79}					
{He I\3/9	884.90}					
{He I\5/11	885.41}					
{[Se III](1F)	885.42}	885.39	3	11.7	10	(a)
{C IV(9-13)	885.74}					
{He II(6-22)	885.91}	885.90	3	43.3	15	(a)
P11	886.28	886.27	3	852.0	3	
X		887.37	3	2.9	40	(c) C II(5d-8f)
X		887.72	3	2.0	35	(c) atm.6%
X		888.54	3	2.3	35	atm.3%
[Fe II](13F)	889.19	889.19	2	14.7	6	
X		889.86	2	2.4	30	(d)
He I\2/7	891.46	891.46	2	5.0	40	(c), (d)
X		892.00	2	2.7	30	(c)
Mg I(25)	892.36	892.27	2	2.3	30	(c)
N V(10-13)	892.57	892.55	2	2.7	30	(a)
{He II(6-21)	892.90}					
{N V(9-11)	892.92}	892.92	2	49.0	5	atm.12%
{He I\10/11	893.06}					
X		893.32	2	1.9	50	(a) atm.5%
X		898.65	2	3.6	40	atm.58%
X		899.26	2	3.2	40	atm.45%

Table 2. (continued)

Identification	λ_{theo}	λ_{obs}	n	$10^4 F/I_\beta$	Error (%)	Comments
{He I\6/10	899.68}	899.71	2	43.3	6	atm.8%
{He I\7/10	899.96}					
X		900.48	2	3.6	35	(a) atm.30%
{He I\5/10	900.90}					
{He II(6-20)	901.12}					
{P10	901.49}	901.51	2	1310.0	13	atm.34%
X		902.17	2	2.3	50	(a) atm.32%
X		902.43	2	3.9	35	(b) atm.34%
{N I(15)	902.89}					
{[Fe II](13F)	903.35}	903.29	2	10.4	30	(b), (d) atm.7%
[Fe II](13F)	905.19	905.20	2	8.8	30	(b) atm.16%
[S III](1F)	906.89	906.89	3	14700.0	15	atm.30%
{C I(3)	907.83}					
{X	}	907.99	2	21.0	30	(a) atm.45%
He I\10/10	908.53	908.49	2	10.5	40	(a) atm.36%
C I(3)	908.85	908.89	2	2.9	50	atm.21%
C I(3)	909.49	909.48	2	12.3	14	atm.21%
X		910.38	2	10.5	50	(b) atm.38%
He II(6-19)	910.85	910.83	3	57.0	10	atm.28%
{He I\9/10	911.09}					
{C I(3)	911.18}	911.17	2	7.0	30	(a) atm.30%
X		911.41	2	2.3	40	(b) atm.30%
O III($4p^3$D-$4d^3F^o$)	911.61	911.72	2	3.3	50	atm.47%
[Cl II](1F)	912.36	912.35	3	48.0	9	atm.11%
O III($4p^3$D-$4d^3F^o$)	913.33	913.38	2	3.7	40	atm.33%
N IV(10.01)	916.51	916.37	2	4.1	25	atm.11%
{O III($4p^3$D-$4d^3F^o$)	917.42}					
{He I\3/8	917.44}	917.48	2	3.2	30	atm.47%
N IV(10.01)	918.22	918.12	2	2.9	30	atm.14%
{He I\6/9	921.02}	921.04	3	65.5	17	atm.10%
{He I\7/9	921.31}					
Mg II(1)	921.83	921.83	2	10.5	50	(b) atm.18%
{N IV(10.01)	922.30}					
{He II(6-18)	922.52}					C II(5f-8g)
{He I\5/9	922.77}					
{P9	922.90}	922.89	3	1940.0	10	atm.35%
{C II(16.02)	922.95}					
{C II(10.02)	923.11}					
C II(10.02)	923.68	923.75	2	9.0	30	(b) atm.25%
Mg II(1)	924.43	924.46	2	7.6	45	(b), (d) atm.23%
{O I(8)	926.09}					
{O I(8)	926.27}	926.20	2	6.7	30	(d) atm.20%
{O I(8)	926.60}					
{[Fe II](13F)	926.75}	926.74	2	11.3	20	atm.30%

Table 2. (continued)

Identification	λ_{theo}	λ_{obs}	n	$10^4 F/I_\beta$	Error (%)	Comments
He I\10/9	930.30	930.36	2	4.0	60	atm.42%
X		931.88	2	5.3	50	C II(5g-8h) atm.61%?
He II(5-8)	934.49	934.50	3	595.0	50	atm.95%?
X		935.40	2	11.7	40	atm.90%?
C III(7.02)	935.84	935.83	2	14.5	50	atm.87%?
He II(6-17)	936.70	936.71	3	92.0	30	(d) atm.67%?
X		938.10	2	10.0	40	atm.40%?
N I(7)	938.68	938.70	1	13.0	50	atm.31%
{[V IV](1F)	940.13}					
{X	}	940.43	2	13.5	30	(d) atm.35%
{C I(9)	940.57}					
X		942.64	2	13.0	40	atm.49%
X		946.04	2	11.7	50	(c) atm.38%
He I\1/5	946.34	946.34	3	78.0	13	atm.38%
X		947.97	2	14.0	35	atm.20%
X		949.30	2	11.0	40	atm.20%
X		949.95	2	16.5	30	atm.20%
{He I\4/7	951.65}					
{He I\6/8	952.60}					
{He I\7/8	952.91}					
{[S III](1F)	953.10}	953.02	1	48400.0	10	atm.15%
He II(6-16)	954.20	954.20	1	150.0	50	(a) atm.22%
P8	954.60	954.52	1	3500.0	15	atm.22%
He I\5/8	955.28	955.25	1	14.0	30	atm.41%
X		957.23	1	11.7	25	(d) atm.3%
He I\10/8	962.56	962.51	1	10.5	30	atm.19%
{C III(2.01)	970.11}					
{He I\3/7	970.25}	970.18	2	11.7	30	(d) atm.6%
{[Ti III](2F)	970.53}					
{C III(2.01)	970.54}					
{C III(2.01)	970.64}	970.60	2	10.5	30	C III(7h-10i)?, atm.3%
{C III(2.01)	971.51}					
{C III(2.01)	971.77}	971.60	2	6.0	50	atm.3%
X		971.95	2	9.5	35	C III(7i-10k)?, atm.3%
He II(6-15)	976.21	976.21	2	99.0	7	atm.11%
[C I](1F)	982.44	982.44	1	243.0	6	atm.4%
[C I](1F)	985.03	985.06	1	725.0	5	atm.4%
{[Kr III](1F)	990.27}					
{C II(17.02)	990.35}	990.39	1	123.0	7	
X		994.25	1	16.5	40	
X		998.02	1	23.0	40	
O II(4fG-5g)	998.24	998.39	1	8.0	60	

Table 2. (continued)

Identification	λ_{theo}	λ_{obs}	n	$10^4 F/I_\beta$	Error (%)	Comments
{O II(4fG-5g)	998.85}					
{O II(4fD-5g)	999.03}	999.02	1	14.0	50	
{O II(4fG-5g)	1000.89}	1000.90	1	8.0	60	
{O II(4fG-5g)	1001.09}					
X		1001.77	2	14.0	30	
{He I\8/7	1002.30}					
{N II(4f'-5g')	1002.33}	1002.31	2	9.5	40	
He I\6/7	1002.76	1002.78	2	147.0	15	
{He I\7/7	1003.10}	1003.14	2	51.0	20	
{N II(4f'-5g')	1003.54}					
He II(6-14)	1004.52	1004.54	2	250.0	30	(a)
P7	1004.94	1004.95	2	4540.0	4	
N II(4f'-5g')	1006.51	1006.32	1	7.0	50	(a)
{N II(4f'-5g')	1007.01}					
{He I\5/7	1007.19}	1007.20	2	11.7	30	
Mg II(4f-5g)	1009.22	1009.15	1	6.0	50	
{N II(65.17)	1010.81}					
{N I(18)	1010.89}	1010.91	2	17.5	30	
{O II(4fF-5g)	1011.04}					
N I(18)	1011.25	1011.24	2	7.0	60	(a)
N I(18)	1011.46	1011.51	2	5.0	90	(a)
He II(4-5)	1012.36	1012.35	2	10500.0	9	
He I\10/7	1013.83	1013.74	1	26.0	25	(a), (d)
C III($5f^1$-$6g^1$)	1016.79	1016.72	1	15.0	50	
X		1017.22	1	56.0	20	
X		1020.34	1	23.0	40	(c)
[Xe III]($^3P_2$-$^3P_1$)	1020.65	1020.63	1	23.0	40%	(c)
He I\9/7	1023.29	1023.32	1	13.0	50	
[Sr IV](^2P-^2P)	1027.69	1027.75	1	15.0	60	
[S II](3F)	1028.67	1028.65	1	1390.0	6	
He I\4/6	1031.11	1031.11	1	106.0	20	
[S II](3F)	1032.04	1032.02	1	1960.0	6	
[S II](3F)	1033.63	1033.62	1	1390.0	7	
{X	}	1036.37	1	40.0	30	
{C II(17.09)	1036.48}					
[S II](3F)	1037.04	1037.04	1	555.0	8	
{[N I](3F)	1039.72}					
{[N I](3F)	1039.77}	1039.78	1	525.0	8	
{[N I](3F)	1040.72}	1040.74	1	365.0	9	
{[N I](3F)	1040.76}					
He II(6-13)	1041.97	1041.97	1	205.0	10	

2.2.3. Sky-emission subtraction

Due to strong emission of the atmosphere, especially in the red and far-red parts of the spectrum where prominent molecular bands are present, sky subtraction is critical because a slight wavelength shift along a CCD row can produce spurious signal due to pixel sampling effects. Reference He and Ar lamp spectra are needed to get an accurate knowledge of the spectrum curvature on the CCD picture. The planetary nebula is de-centered in the field of the spectrometer slit in order to get a sky region where the central wavelength, for a given CCD row, is identical to that of the corresponding pixels within the nebula. The atmospheric emission spectrum is obtained from the sky data after removing spikes and averaging over a sufficient number of CCD columns, in order not to degrade the signal-to-noise ratio of the nebular spectrum. For bright standard stars, less affected by atmospheric emission due to short exposure time, the sky emission is directly measured on the CCD picture on both sides of the star spectral track.

2.2.4. Sky absorption correction

The wavelength shifts are treated as in Sect. 2.2.3. Information on the sky absorption spectrum is obtained from observation of bright stars with no spectral feature of their own. After scaling the atmospheric absorption to the corresponding air masses, the correction is applied to the nebular spectrum. The efficiency of this procedure is mainly limited, in strong absorption bands, by our ability to get exactly the same central wavelength for each spectral element on the star and on the nebula. Furthermore the fact that the atmospheric absorption lines are much narrower than both the spectral resolution and the nebular lines is also limiting the accuracy of this procedure where nebular emission lines are present: this is taken into account in the error estimate of nebular line intensities (Sect. 3.2).

2.2.5. Wavelength and flux calibration

Since many nebular lines, particularly H I and He II, have well-defined wavelengths and are quite regularly spread over the spectral range of interest, they are used to provide the wavelength calibration function. In regions where such lines are lacking, we use those forbidden lines which have accurately defined wavelengths. The accuracy of the wavelength determination is from 0.02 nm for bright lines to 0.05–0.10 nm for the faintest lines.

The flux calibration is achieved by means of secondary standard stars (Oke & Gunn 1983). The spectral data are summed over a large number of CCD columns in order to provide a correct spectrophotometry even though this increases the noise level which however remains below 1% in a majority of cases. Then, after correcting for atmospheric absorption, a third-order polynomial fitting is applied to provide the relative flux calibration curve over the spectral range covered by the CCD, using the absolute spectral energy distributions given by Oke & Gunn (1983). Above 1000 nm, bright stars are measured in order to shorten the exposure time. Their spectra are calibrated using absolute data on Vega (Oke & Gunn 1983). The calibration uncertainty is estimated from the scatter of the results within a set of standard star spectra at a given wavelength. A conservative figure of 3% is adopted. Of course the quality of the calibration is degraded at wavelengths greater than about 900 nm, due to reduced detector sensitivity and increased fringe contrast.

2.2.6. Final spectral scaling

Observations were secured with large overlap of consecutive spectra. After reduction and relative calibration, the spectra are adjusted using arbitrary multiplicative factors to yield continuity on the nebular continuum throughout the regions of overlap. In order to check for possible cumulative effects, the spectral coverage being nearly one octave in wavelength, low-resolution spectra taken in 1988 (Table 1) were also measured. The low- and high-resolution spectra turned out to be consistent within 4% after independent calibration. This agreement gives confidence in the calibration procedure adopted in this work. After calibration, the intensities in "counts" per pixel are proportional to energy fluxes (Paper I).

3. Identification of lines and intensities

3.1. Presentation

The results are presented in Table 2. Col. 1 gives line identifications with multiplet numbers in brackets (Moore 1965, 1970, 1971, 1975, 1976, 1979, 1980, 1983, 1985). Unidentified lines are noted "X". The theoretical wavelengths of the lines are given in col. 2 (Moore's compilations; Martin et al. 1988; Fuhr et al. 1988; Kaufman & Sugar 1986; Sugar & Corliss 1985; Kaufman & Martin 1991, and references therein; Johansson 1978; Petterson 1982; Wenaker 1990; see also a list of references in Table 1 of Paper II for heavy elements).

Some wavelengths, computed from energy levels of Moore and others but with no multiplet number, are explicitly defined by their lower and upper levels. For the He II transitions, the lower and upper principal quantum numbers appear in brackets in col. 1. For the quasi–hydrogenic transitions of multi–charged ions such as C IV and N V, the same notation as for He II is adopted when no multiplet number is available. The notation used here for the He I lines with lower principal quantum number $n = 3$ is explained in Table 3 and is the same as in Paper I: for example, He I\6/13 is the line $n = 13$ of series number 6 (namely series 3^3D–n^3F, also noted "S6" in Paper I). Other He I lines are noted by means of their multiplet number.

Transitions involving extrapolated energy levels and mentioned as "comment" in col. 7 will be discussed in Sect. 4.5.

In col. 3 of Table 2 is given the observed wavelength and in col. 4 the number of independent measurements from which the line intensity of col. 5 was derived.

In col. 5, the intensity F_λ is in units $I_\beta = 10^4$. This intensity is *not* corrected for interstellar extinction and results from a direct scaling of the kind described in Sect. 2.2.6, using unpublished optical spectra connecting Hβ to Hα (Paper V).

Table 3. He I series

Label	Transition	Label	Transition
He I\1/n	3^1S-n^3P	He I\6/n	3^3D-n^3F
He I\2/n	3^1S-n^1P	He I\7/n	3^1D-n^1F
He I\3/n	3^3P-n^3S	He I\8/n	3^1D-n^1P
He I\4/n	3^3P-n^3D	He I\9/n	3^1P-n^1S
He I\5/n	3^3D-n^3P	He I\10/n	3^1P-n^1D

De-reddened intensities *relative to* Hβ will be noted I_λ. The reddening correction is considered in Sect. 4.4.

The estimated error (in % of line intensity) is given in col. 6 (Sect. 3.2).

3.2. Error analysis

The error given in col. 6 of Table 2 results from several factors encountered during the data treatment. They are listed below together with indications about the way they were assessed and their impact on the overall error.

The measurement noise is intrinsic to the detector used for the observations (either RCA or Thomson CCD's). In addition to the read-out noise it also includes the error due to the flat-fielding correction. The latter source of noise is largely dominant beyond 900 nm for the RCA CCD's.

Sky subtraction may induce large errors at wavelengths where a strong sky emission line is present. The procedure adopted in Sect. 2.2.3 intends to minimize this error. Special attention was devoted to the few strongest telluric emission lines. In most cases this error is smaller than the measurement noise.

The error due to the atmospheric-absorption correction is obviously related to the amount of absorption. The mean atmospheric absorption at the wavelength of a line is given in col. 7 of Table 2 (noted "atm.", in %), when it exceeds 3%. In domains of strong atmospheric absorption, the noise level is dominated by the absorption correction uncertainty (Sect. 2.2.4) and the global error given in col. 6 is often relatively large.

The underlying continuum may be ill defined in the wings of some strong nebular lines, particularly when they are saturated in the CCD image and confusion may arise from dragging effects. The shape of the wings is found to strongly depend on the CCD used and the degree of saturation. This uncertainty is tentatively taken into account in estimating the overall error, particularly for faint lines.

The actual continuum may also be affected by the crowding of several faint lines but this is difficult to quantify.

In case of critical blend or overlap, the overall intensity of the feature is given in Table 2 for the sake of accuracy. An estimate of the relative intensity of individual components can often be obtained when necessary (Paper IV).

At last, the flux-calibration error induces relative flux uncertainties on lines separated by a large spectral interval. The fact two independent calibrations match together within 4% (Sect. 2.2.6) over the whole spectral range suggests an overall absolute uncertainty of this order (not included in the estimate of col. 6).

Most comments appearing in col. 7 deal with sources of uncertainty. A few standard comments are noted by means of letters as follows: (a) the line belongs to the wing of a strong line; (b) the continuum under the line is not accurately defined; (c) the line intensity is obtained after de-blending from nearby lines of roughly similar intensity; (d) the line is broad and no de-blending is applied (however code (d) is omitted for "standard" blends, see Sect. 4.1.1).

4. Comments

4.1. Statistics

4.1.1. Lines

The total number of lines (including the X's) listed in col. 1 of Table 2 is 654. Out of the 48 lines appearing in col. 7 (Sect. 4.5), 26 are blended with otherwise identified features and 22 effectively replace 22 X's of col. 1, so that the grand total of *different* lines listed in Table 2 is 654+26 = 680. However many lines are blended, notably the helium lines at the end of the Paschen series, and the number of "truly" distinguishable lines is smaller.

405 features were given an intensity in col. 4 of Table 2. The "effective" number of detected lines is larger since, for the sake of accuracy of the listed intensities, many blends, obvious on the tracings, were not explicitly de-blended. For example, the wings of most Paschen lines are clearly enhanced notably by He II and He I lines and approximate intensities can be obtained from observation. The effective number of *detected* lines is therefore taken as the number of features in col. 4, with the convention that broad features for which no de-blending was attempted (noted "(d)" in col. 7) are equivalent to 1.5 or 2 different emission lines. The weight 1.5 is adopted in case the feature is judged weak and/or practically difficult to de-blend. Although they were not noted (d) in col. 7, Paschen lines are considered as two independent features in all cases their wings are detectably enhanced by He II lines (among other lines). The same remark applies to the clear blend of series He I\6/n and He I\7/n (Paper I), inasmuch as they are not lost in the Paschen series (see an example in Fig. 15 of Paper II: features "i" and "j" are grouped together in Table 2). Using this somewhat subjective rule, there are ~465 observationally-distinguishable lines.

Some care has been exercised at checking the consistency of the proposed identifications as often as possible (Paper IV). Nonetheless the fact a theoretical wavelength coincides with an observed one within uncertainties is no warranty the identification is correct or complete, especially for weak lines.

The "truly unidentified lines" (hereafter "unidentified lines") are those lines noted "X" in col. 1 of Table 2, which were not given an identification in col. 7 (Sect. 4.5). There are 62 such lines, that is 13% of the 465 different lines detected.

Table 4. Line-flux measurement limit[a]

Δλ(nm)	F_λ^{min}	I_λ^{min}	Remark
654 – 686	0.8	0.25	
686 – 696	1.3	0.40	H_2O
696 – 717	1.0	0.30	
717 – 727	3.0	0.80	H_2O
727 – 759	0.8	0.20	
759 – 768	4.0	0.90	O_2
768 – 812	0.8	0.15	
812 – 826	2.0	0.35	H_2O
826 – 856	1.8	0.30	Paschen
856 – 886	1.4	0.20	
886 – 893	1.5	0.20	
893 – 903	2.5	0.35	H_2O
903 – 933	5.0	0.70	H_2O
933 – 970	10.	1.20	H_2O
970 – 1012	10.	1.10	
1012 – 1045	18.	1.90	

[a] Intensity F_λ and de-reddened intensity I_λ in units of $10^{-4} I_\beta$.

4.1.2. Errors

About 1/4, 1/2, and 2/3 of the ~400 intensities listed in Table 2 have quoted errors $< 10\%$, $\leq 25\%$, and $\leq 30\%$ respectively.

About 30 lines are listed, whose intensities are affected by errors greater than 50%. In general these very uncertain features are considered only insofar as they coincide with missing lines of otherwise observed multiplets. Due to this bias, virtually all of them are necessarily "identified".

About 60 lines are mentionned with an error of 50%, out of which 15 are unidentified. The fraction of unidentified lines (1/4) is somewhat larger than on average, owing to the difficulty to fully describe theoretical spectra down to very weak lines.

4.1.3. Flux-measurement limit

The measurement limit is defined in practice as the minimum line intensity allowing a measurement with an error not exceeding 50%. It is estimated that less than 10% of the lines quoted with this large an error are spurious detections. The detection yield may be ~3/4 close to the limit, approaching 100% for intensities twice larger than the limit. Mildly reliable *detection* (with very large uncertainty) is still possible for fluxes ~1.5 times weaker than the measurement limit.

There are obvious provisos to the above statements. First, weak lines are unreachable in the vicinity of strong lines due to saturation and leakage. The interval affected by a strong line is generally not symmetrical about the line wavelength and depends on the line strength, CCD characteristics, spectral resolution, and exposure time. Second, the detection limit worsens in a more or less erratic manner within atmospheric absorption bands.

Table 4 provides approximate measurement limits for spectral ranges listed in col. 1. The F_λ limit is given in col. 2 and the (de-reddened) I_λ limit in col. 3 (Sect. 4.4). Inside atmospheric bands, the quoted limit should be understood as some kind of an "effective average", detection being very difficult at selected wavelengths.

Table 5. Line detection and identification

Δλ(nm)	KACE	KAF	Present	
654 – 823 nm				
Line number	29	43	249[a]	(220)[b]
Unid. lines	3	14	23	
$< F_\lambda >^{c}_{unid}$	120	48	2.3	
823 – 875 nm				
Line number	17	48	84	(63)
Paschen lines	14	25	27	
Other lines	3	23	57	(36)
Unid. lines	2	11	8	
$< F_\lambda >_{unid}$	70	26	5.8	
875 – 1045 nm				
Line number	14[d]	–	129	(119)
Unid. lines	0	–	30	
$< F_\lambda >_{unid}$	–	–	11.5	

[a] Number of detected lines.
[b] Number of explicit intensities in Table 2.
[c] Mean intensity of unidentified lines ($I_\beta = 10^4$).
[d] Compilation.

Shortward of 826 nm, the measurement limit is normally $F_\lambda \sim 0.8$–1 in our units, except for three atmospheric bands ~10 nm wide. The corresponding de-reddened limit I_λ runs from ~0.30 (660 nm) to 0.15 (820 nm). The F_λ limit is twice as bad in the interval 826–900 nm, due in part to the difficulty in accurately defining the continuum level in between the many hydrogen and helium lines (in addition even relatively strong lines are hard to see close to the end of the Paschen series). However the I_λ limit is about the same as above. Thus, over ~200 nm, that is 80% of the interval 654–900 nm, lines are effectively detected and measured down to $(1–2)\times 10^{-6}$ of [O III], the strongest optical line. The detection limit is degraded throughout the atmospheric H_2O band 893–980 nm, particularly beyond 900 nm, and does not recover at longer wavelengths owing to the lower sensitivity of the detector and the smaller number of spectra available.

4.2. Comparison to previous surveys

Previous spectral surveys encompassing at least part of the range considered here include those by Aller & Minkowski (1946), Kaler et al. (1976, hereafter KACE), Condal et al. (1981), and Keyes et al. (1990, hereafter KAF). The line list of Condal et al. (1981) is almost identical to that of KACE and will not be considered. In retrospect one should acknowledge Aller & Minkowski (1946) decisively established the field since their pioneering list of ~30 far-red lines has not been significantly

Table 6. Identifications in KAF

λ(nm)	Identification
685.0	[Mn VI]
705.4	O IV + [Cr IV]
705.9	wg He I: O IV
706.2	wg He I: He I + C IV
728.2	He I
748.7	C III
749.3	spurious
753.5	[Xe IV]
770.3	N IV
771.3	O IV
772.4	Si IV + O IV
772.6	C IV
773.6	C IV
819.7	C III
825.0	P40 + P39 + O III
825.5	P38
825.8	P37
834.2	wg P23: He I + He II
834.8	wg P23: He II
850.0	wg P16: [Cl III]
859.4	wg P14: He II
861.7	[Fe II]
866.7[a]	wg P13: He II
873.3	He I + He I
874.7	wg P12: He II

[a] Probable misprint: read 866.1.

superseded until the late 80's, excepting a dozen rather trivial Paschen lines.

4.2.1. Detection rates

Table 5 compares statistical information about lines detected by KACE, KAF, and in the present work for the three spectral ranges 654–823 nm, 823–875 nm, and 875–1045 nm, where λ823 nm corresponds to the effective limit of the Paschen series and λ875 nm to the maximum wavelength observed by KACE and KAF. For the range 875–1045 nm, the column "KACE" corresponds to their compilation of pioneering photoelectric measurements by O'Dell (1963) and Schwartz & Peimbert (1973), to which are added the 3 lines [C I] discovered by Danziger & Goad (1973).

For each spectral range is given (1) the total number of observed lines, (2) the number of "unidentified" lines (including a mis-identification of λ772.6 in KACE and KAF, Sect. 4.5.2), and (3) the mean intensity $< F_\lambda >$ of the unidentified lines (in units of $10^{-4} I_\beta$). For the interval 823–875 nm, the observed lines are further subdivised into Paschen lines and other lines.

4.2.2. Wavelength range 1: 654–823 nm

Out of the 3 unidentified lines in KACE, one was a C III line, another one was in fact mis-identified ([S I] instead of C IV), and the last one, λ808.8, was probably a spurious detection (although it was listed by Condal et al. with even larger intensity). Note that the lists of lines in Aller & Minkowski (1946) and KACE were very similar, whereas the relative line intensities were in reasonable agreement.

KAF increased the number of detections by 50%, but proposed almost no new identification, so that 1/3 of all lines were left unidentified. Most of these new lines are now probably identified (Table 6) except for λ749.3, that we do not see (upper limit 1.5 in our units). Also, our intensities for λ660.1 and λ815.6 are about 1/10 and 1/3 those of KAF, respectively, that is below their detection limit. Thus ∼27 lines are really observed *and* identified by KAF in range 1, to be compared to the ∼226 such lines quoted in Table 2 in the same range.

The fraction of unidentified lines is ∼1/10 in Table 2. The drastic decrease of the mean intensity of unidentified lines (Table 5) from KAF to the present work confirms that the improvement in either detection limit or identification rate amounts to one order of magnitude.

4.2.3. Wavelength range 2: 823–875 nm

Out of the 3 non-Paschen lines quoted by KACE, one, λ827.0, roughly coincide with the excess observed in P34-P36 (Paper I) but may as well be spurious since it was not mentioned by KAF, another one was mis-identified ([Fe II] instead of O I), and the last one was correctly identified, except for a rather inaccurate wavelength and a typing error ([Cl III] should read [Cl II]).

In range 2, the use of a CCD was a breakthrough since KAF detected twice as many Paschen lines as did KACE and many non-Paschen lines. However half the new lines awaited an identification (Table 6). Due to the many Paschen lines, the number of potentially detectable non-Paschen lines is somewhat reduced. Nonetheless, compared to KAF, the detection rate is more than doubled in the present work, while both the identification rate of non-Paschen lines and the mean intensity of unidentified lines are improved by nearly a factor of 5.

4.2.4. Wavelength range 3: 875–1045 nm

Since the photoelectric measurements compiled by KACE, only a handful of new detections and identifications were reported in range 3 for NGC 7027 (e.g., Rudy et al. 1992). In Table 2, the number of lines is increased by one order of magnitude.

Despite this improvement, the detection rate per unit energy interval is ∼50% smaller than in previous ranges. About 40% of range 3 is severely affected by H_2O absorption, while the sensitivity of the detector is lower.

4.2.5. Line intensities

Figures 1–5 show the logarithmic differences between previous and present measured intensities (*relative to* Hβ). Figures 1 and 2 compare the KACE intensities with ours in range 1 (654–823 nm) and range 2+3 (823–1045 nm), respectively. For the comparison with KAF, range 1 is split in two intervals:

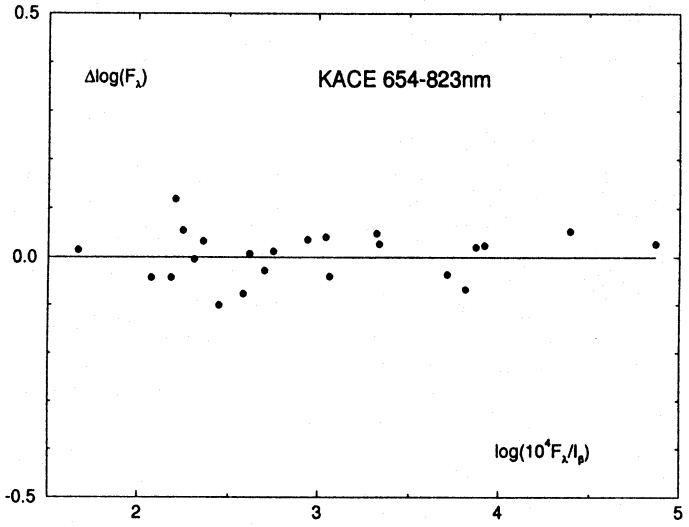

Fig. 1. Logarithmic differences between the intensities listed by Kaler et al. (1976) and those of Table 2 versus the log of the intensities of Table 2 for the wavelength range 654–823 nm. The line λ808.8 listed by KACE is omitted

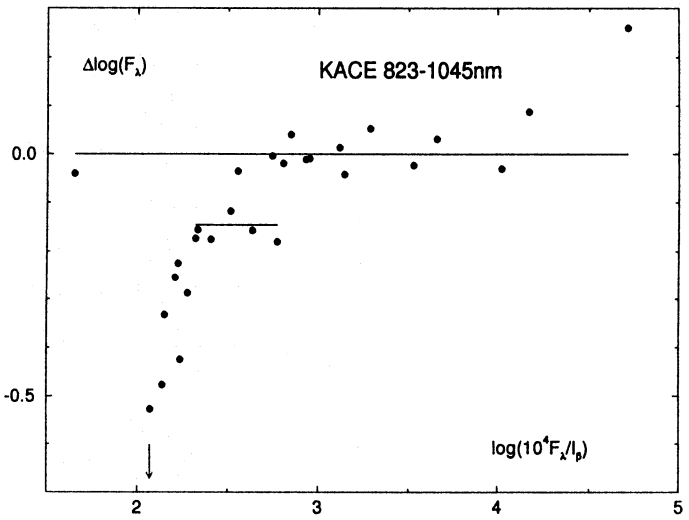

Fig. 2. Same as Fig. 1 for the range 823–1045 nm. Points to the right of $x \sim 2.75$ (intensities $\geq$ 600) correspond to pioneer photoelectric measurements. Other points correspond to KACE's photographic measurements of Paschen lines ($\lambda \leq 867$ nm). The low-intensity isolated point correponds to λ827.0 (KACE), tentatively associated to the flux excess in P34–P36 (Paper I). Points corresponding to P25 and P26 lie in the direction of the vertical arrow. The short horizontal segment is shifted down from $\Delta \log F_\lambda = 0$ by a factor 1.4 and runs across the points corresponding to P13–P18

Figures 3 and 4 correspond to intervals 654–740 nm and 740–823 nm, respectively, and Fig. 5 to range 2 (823–875 nm). The horizontal scale is in $x = \log(10^4 F_\lambda / I_\beta)$, using the data of Table 2.

No departure from linearity and no difference in scaling relative to Hβ is apparent shortward of the Paschen limit (range 1), comparing with either KACE (Fig. 1: 3.5 decades in intensity) or KAF (Fig. 3: 4.5 decades and Fig. 4). However Fig. 4 shows that, longward of 740 nm, the intensities of KAF are larger than ours for lines with $F_\lambda \leq 15$ in our units ($x \leq 1.18$). In Fig. 3, the two points $x \leq 1.0$, the feature λ660.1 which lies out of the graph, and the striking gap $1.0 \leq x \leq 1.5$ are all consistent with the trend seen in Fig. 4. That an intensity of 15 is close to the detection limit of KAF is also suggested by the fact, in the full range 1+2, KAF missed about 20 lines with $F_\lambda \geq 10$, whose mean intensity is 16 (excluding the very strong [C I]872.7, forgotten by KAF).

In Fig. 2, the limit between photoelectric and photographic measurements (scaled by photoelectric data) of KACE approximately corresponds to an intensity of 600 ($x = 2.75$). Old photoelectric data compare quite well with our results, except for the strongest line [S III]953.1 (O'Dell 1963), which indeed proved to be overestimated: Scrimger et al. (1978), Dinerstein (1980), and Condal et al. (1981) obtained values within 10% of ours.

In Fig. 2, the photographic data of KACE almost exclusively encompass the end of the Paschen series (P13–P25). From P13 to P18, the KACE intensities are shifted downward by a roughly constant factor of 1.4 (the O'Dell flux for P13 turned out to be correct but was unfortunately not used by KACE to scale their long-wavelength intensities, possibly because some inconsistencies appeared at shorter wavelengths). Then the "asymptotic" shrinking of KACE intensities relative to ours beyond P18 (factor $\sim 4 \times 1.4$ at P25 and P26, which lie out of Fig. 2) is probably not due to a departure from linearity but indicates that KACE measured intensities above some "effective" continuum, which depends on both the spectral resolution used and the progressive blending of the lines. The continuum we adopt at the end of the Paschen series is a straightline extrapolation from longer wavelengths (Paper I).

Discrepancies qualitatively similar to those revealed in Fig. 2 are apparent on comparing the KAF intensities with ours (Fig. 5). First, although there is a rather tight correlation over the upper decade of the graph, the KAF intensities are shifted downward by a constant factor of $\sim$1.19. Second, a shrinking of their Paschen-line intensities is detectable beyond P28. In fact a sharp jump between P30 and P31 and a roughly constant shift $\sim$1.5 of the P31–P38 intensities listed by KAF with respect to the present ones is also consistent with the data.

The problem at the very end of the Paschen series may again be one of definition of the continuum level. Thanks to a better spectral resolution and signal to noise, KAF results (Fig. 5) remain parallel to ours up to P29-P30 ($x > 1.80$) instead of P18 ($x > 2.25$) in the case of KACE (Fig. 2). Also the departure of KAF intensities from ours beyond P30 is much less severe than before.

The good correlation between both the recent CCD sets of intensities for most relatively strong lines is encouraging. On the other hand, the shift of 19% in Fig. 5 is not understood. It may partly arise from the fact the intensities of strong lines in Table 2 include contributions from weaker helium lines. We note however that (1) the total of these contributions most often amounts to 3–8% of the Paschen lines, (2) not all of these

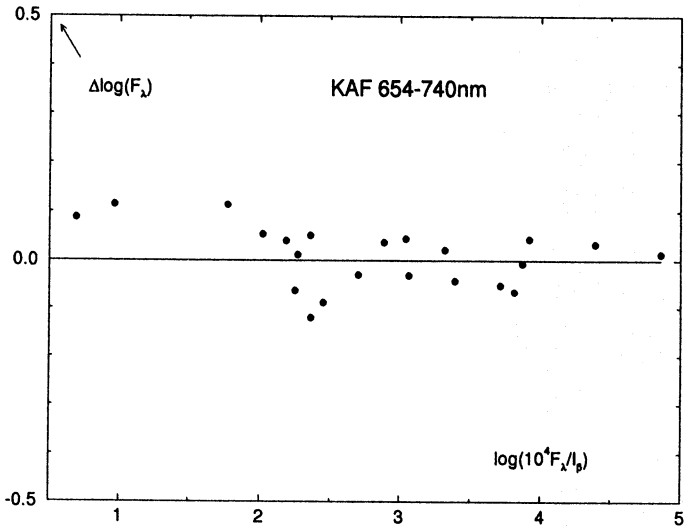

Fig. 3. Logarithmic differences between the intensities listed by Keyes et al. (1990) and those of Table 2 versus the log of the intensities of Table 2 for the wavelength range 654–740 nm. The point corresponding to line λ660.1 lies in the direction of the left-corner arrow

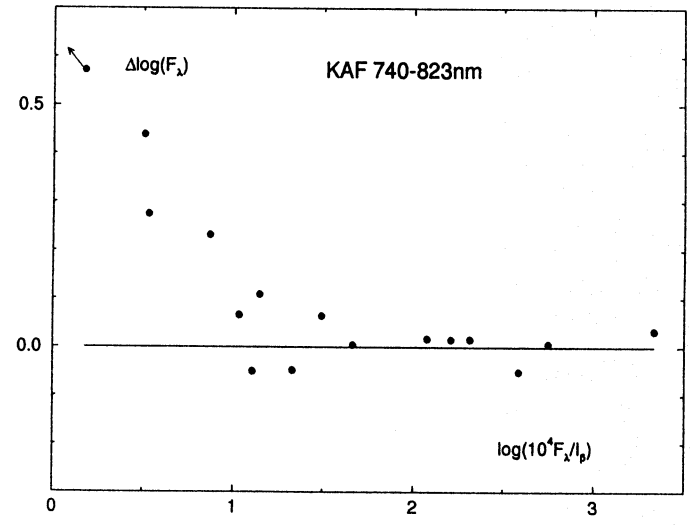

Fig. 4. Same as Fig. 3 for the range 740–823 nm. The point to which is attached an arrow corresponds to our upper limit to the intensity of λ749.3

contributions can be distinguished and removed observationally, and (3) all lines listed by KAF in the vicinity of a strong line were added to the strong line before comparing to our data. This discrepancy cannot be due to some more or less continuous drift of calibration with wavelength since no tendency at all is seen in Figs. 3 and 4. Therefore a quasi discontinuity must exist within the interval 820–823 nm, that is at the Paschen limit, in one of the data sets. Our data and procedure exclude, we think, an error exceeding ~3%. We note that this shift almost exactly coincides with the "implicit" shift between the present data and those we published earlier in Paper I for H and He lines over the range 681–1045 nm (Sect. 4.4.1). This should be coincidental,

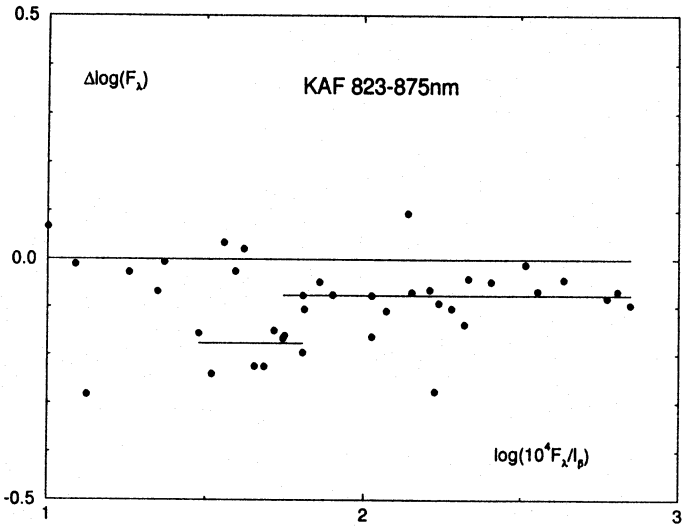

Fig. 5. Same as Fig. 3 for the range 823–875 nm. The long segment is shifted down from $\Delta \log F_\lambda = 0$ by a factor 1.19 and runs across the points corresponding to $x \geq 1.75$ (intensities ≥ 60). The short segment is shifted down by a factor 1.5 and runs across the points corresponding to P31–P38 (see Sect. 4.2.5)

as KAF did not refer to the intensities of Paper I to calibrate their own intensities longward of the Paschen limit.

4.3. Unidentified lines

4.3.1. Most significant lines

A majority of the ~60 ("truly") unidentified lines in Table 2 are very weak.

27 unidentified lines are found with an error not exceeding 30%, out of which 9 have intensities larger than 10 in our units. However, 5 among these 9 lines belong to restricted spectral intervals (particularly 940–958 nm) badly affected by atmospheric absorption, in which the error estimate itself is dubious.

About 10 unidentified lines are found with an error not exceeding 20%. Among them, only two, namely λ838.72 and λ1017.22, stands out in that their intensities are significantly larger than 10 in our units.

De-reddened intensities are physically more significant, especially as reddening helps to compensate for the decrease of sensitivity toward long wavelengths. Using to a first approximation the reddening law of Paper I (Sect. 4.4), only 4 unidentified lines are found with an intensity $I_\lambda \geq 3 \times 10^{-4} I_\beta$ (λ907.99, λ1036.37, in addition to the above lines). Also 15 have either $I_\lambda \geq 0.9 \times 10^{-4} I_\beta$ or an error less than 20%, but only 6 of them fulfill both criteria (λ695.87, λ771.95, λ816.02, λ863.36, and again λ838.72, λ1017.22).

4.3.2. Wavelength distribution

The mean intensity of unidentified lines is roughly doubling from one wavelength range to the next (Table 5). The difference between ranges 1 and 2 may not be very significant as the mean

would be decreased by a factor 1.6 in range 2 on removing just line λ838.7. Conversely other relatively strong unidentified lines may easily be "hidden" by the several Paschen lines showing an excess intensity (Paper I), then increasing the mean intensity quoted for range 2. It remains that the variation from range 1 to range 3 is certainly significant: as expected, the unidentified lines are stronger in lower signal-to-noise conditions.

However what may not be expected is that the fraction of unidentified lines in range 3 is ∼1/4, compared to a constant value ∼1/10 in the rest of the spectrum. Some explanations may be as follows:

1/ Due to insufficient spectral resolution, the correction for atmospheric absorption is on occasion so unreliable as to produce spurious lines (with some kind of consistency). This is certainly a serious problem, although we have tried to be reasonably selective in accepting lines in such cases. Note that, within the H_2O band, say 893–963 nm, neither the fraction of unidentified lines nor their mean intensities seem particularly enhanced.

2/ More spurious lines are generated at longer wavelengths, due to the lower signal-to-noise ratio. In principle the criteria leading to line detection are the same at all wavelengths and should not produce such an effect.

3/ Most unidentified lines are real in range 3 and atomic spectra are less thoroughly described at longer wavelengths. Although the observations are of lesser sensitivity, this is our preferred interpretation. Emission at long wavelengths may a priori involve many atomic levels, particularly from complex ions, such as C I, N II, O II, O III in which the details of radiative cascades following recombination are not well known (departure from LS coupling, etc). One more difficulty is that, due to the lower rate of detection, many lines useful to check the presence of multiplets may be missing.

4.4. Reddening and Paschen lines

4.4.1. Previous reddening corrections

The conversion of far-red relative intensities into intensities relative to Hβ was obtained in Paper I by means of theoretical intensities of Paschen lines, assuming (1) mean physical conditions derived from a photoionization model of the nebula *and* (2) a standard reddening law, as formulated by Miller & Matthews (1972), with a logarithmic extinction at Hβ of c = 1.40 and a ratio of total to selective extinction $R = A_V/E_{B-V} = 3.20$ (R recommended by Seaton 1979b; later in this Section, following a remark by Howarth (1983), we shall adopt the reddening law as formulated by Seaton 1979a, with $R = 3.1$).

This indirect "absolute" scaling was used in Paper II to get far-red line intensities from heavy elements, as the final connection to the optical was not yet achieved.

The intensities given in Table 2 are 17% larger than those corresponding to the scaling made in Paper I. This difference is to be compared to the 4% uncertainty introduced in the process of connecting the far red to Hβ through successive continuum overlaps (Sect. 2.2.6). Unless the physical conditions assumed in Paper I were unrealistically wrong (see a discussion of the sensitivity of the Paschen decrement and Paschen discontinuity to physical conditions in Paper I), this difference would suggest that the reddening correction adopted in Paper I (and Paper II) was somewhat too small. Using the same reddening law, coherence between Paper I and the present data would be restored at $\lambda = 840.0$ nm if one would accept c = 1.53.

The reddening correction to be applied is a subject of debate (Miller & Mathews 1972; KACE; KAF). Differences between authors and methods, which roughly amount to ±0.1 on c, are likely to be real, reflecting the uneven distribution of dust absorption across the nebula (Atherton et al. 1979; Seaton 1979b; Condal et al. 1981). The value c = 1.40 (Paper I) intended to be a reasonable average value. On the other hand, the value c = 1.53 is larger than any global determination so far and leads, from Table 2, to $I_\alpha/I_\beta = 2.44$, which is inacceptably low compared to the theoretical value of 2.78.

Notice that, in Paper I, the reddening correction was only applied *differentially* within the far-red range. As long as the recombination theory for H (and He) is correct and the adopted mean physical conditions were roughly acceptable, the dereddened intensities of most far-red lines considered in Paper II could hardly be in error by more than 10%, irrespective of the actual reddening law (see below).

4.4.2. Uneven distribution of reddening

The uneven distribution of reddening across the nebula has been re-considered by Walton et al. (1988), who compared Hβ maps to radio maps, Woodward et al. (1992), who analysed colour excess from H and K images, and Robberto et al. (1993), who performed sub-arcsecond optical line imaging. Reddening can greatly vary on a relatively small angular scale, so that the use of one simple reddening law to connect, e.g., the far-red to the optical may be questionable, when dealing with spectra averaged over different parts of the nebula (Seaton 1979b; Middlemass 1990).

Our North-South slit encompasses the "bright spot", which corresponds to a minimum of reddening, and the conspicuous South-West part of the heavily reddened, sharply defined, "equatorial disk", best visualized in the [O III]/Hα image (Fig. 8 of Robberto et al., almost equivalent to an Hβ/Hα image). Using the Hβ/Hα ratio of Robberto et al. (1993), these two regions correspond to $A_V \sim 2.4$ ($E_{B-V} \sim 0.79$) and $A_V \sim 3.5$ ($E_{B-V} \sim 1.13$) respectively. Using instead [O III]/Hα, which provides a much better signal-to-noise ratio, the variation of E_{B-V} from the bright spot to the equatorial spot is 0.69, that is twice larger than the one deduced from Hβ. A differential extinction $E_{B-V} \sim 0.8$ is in general agreement with optical, infra-red, and radio data for the bright spot (references above). Then, based on [O III]/Hα, E_{B-V} should be 0.8 + 0.7 at the equatorial spot, that is almost twice larger than at the bright spot. This estimate is based on optical data only. A ratio of E_{B-V}'s even larger than 2 can be anticipated in a comparison of far-red lines to Hβ since more heavily obscured zones, not sampled at optical wavelengths, may be progressively revealed at longer wavelengths through the equatorial disk. Although somewhat more ambigu-

ous, the map of the $H-K$ colour-magnitude excess confirms this trend: an absolute maximum of reddening clearly appears in the south equatorial zone crossed by our slit, where E_{B-V} may be 3 times larger than in the bright-spot zone (Fig. 5 of Woodward et al. 1992) and the visual extinction may locally reach $A_V \sim 8$. According to Woodward et al. (1992), this is in approximate agreement with the extinction map derived by Atherton et al. (1979) from the ratio of Hα to 5 GHz continuum emission.

From these observations, it is concluded that: (1) the *intrinsically* brightest parts of the nebula encompassed by our slit can be divided into two relatively well-defined zones (zone 1 = visual "bright spot" and zone 2 = "equatorial disk"), (2) the E_{B-V} relevant to a comparison of the optical to the far-red emission may vary by a factor 2 to 3 from zone 1 to zone 2, and (3) zone 1 corresponds to a typical (minimum) $E_{B-V} \sim 0.8$.

The observed ratio F_α/I_β of Hα to Hβ in the slit is 7.37 (Table 2) and the intrinsic ratio is $I_\alpha/I_\beta = 2.78$ (using case B recombination, T = 1.45 10^4K and $n_e = 6\times10^4 cm^{-3}$, Hummer & Storey 1987). Assuming a completely uniform reddening within the slit, the differential extinction is $E^0_{B-V} = 0.911$ (Seaton 1979a, with $R = 3.1$).

Consider a schematic 2-zone model in which E_{B-V} is uniform in each zone. Assume the *intrinsic* relative line fluxes from both zones are equal. Let a be the fraction of intrinsic flux within the slit produced in zone 1. Given E^1_{B-V} ($< E^0_{B-V}$) and E^2_{B-V}, a is uniquely determined by the condition $I_\alpha/I_\beta = 2.78$.

Taking for example (see above) $E^1_{B-V} = 0.8$ and $E^2_{B-V} = 2.0$, zone 1 is found to produce $a = 26\%$ of the intrinsic emission and 95% of the Hβ flux *observed* in the slit. Compared to the strictly uniform (one zone) model with $E_{B-V} = E^0_{B-V}$, this 2-zone model increases the reddening-corrected intensity relative to Hβ (and Hα) by 11.4% and 25.8% at 840 nm and 1000 nm respectively.

Although rather extreme, this example illustrates qualitatively how a strongly varying obscuration across the slit, independently documented in many observations, can help reconciling the present data with the theoretical scaling performed in Paper I (assuming uniform reddening).

A problem faced in Paper I was an apparent excess of intensity of the upper part of the Paschen series (principal quantum number $n > 21$, $\lambda \leq 837$ nm) relative to the lower part. In Paper I, this problem led to the assumption that many high-n Paschen lines should be blended with unidentified lines. Indeed a number of such blends is now identified (Table 2), reducing substancially the intensity of many of the "anomalously" strong lines (Paper IV). Nonetheless, a significant excess is still globally present. As shown above, this excess may be removed after considering explicitly non-uniform reddening and can be taken as a spectroscopic signature of non-uniform reddening.

4.5. Permitted lines

4.5.1. Extrapolated levels

A number of unidentified lines is attributed to transitions involving a level whose energy was extrapolated by us from available information: then the transition is defined in col. 7 ("comments") and no "theoretical" wavelength is given in col. 2 or 7. When a new transition is defined in col. 7, it should be understood that the observed wavelength (col. 3) agrees with the extrapolated value within usual uncertainties. However a question mark is attached to the identification in case the extrapolated wavelength is judged inaccurate. Two question marks mean the wavelength is very tentative and the identification is at best a suggestion.

Many quasi–hydrogenic transitions, which were also introduced by us, particularly for C IV, O IV and N V, are expected to be sufficiently well determined to appear in col. 1 and 2 with no special comment.

A few dielectronic lines are only known from theory (Nussbaumer & Storey 1984): they appear in col. 1 but a question mark is attached to their wavelength in col. 2. In some cases an "empirical" wavelength based on the observed spectrum is proposed in col. 7.

Owing to the large abundance of carbon in NGC 7027, many permitted lines from all possible ions of carbon show up. A few qualitative aspects of line identification are now discussed, emphasizing the carbon lines obtained by extrapolation of level energies and some consequences for the optical range. Quantitative aspects are postponed to Paper IV.

4.5.2. C IV

The line λ772.62 was identified with [S I] by KACE and KAF, even though the wavelength coincidence was known for some time to be poor (Eriksson 1978). The very large strength of this presumed forbidden line has been a subject of concern (Péquignot et al. 1978; Butler & Dalgarno 1980), casting undue doubts on the correctness of conclusions based on detailed modelling of nebulae. In the present observations, the variation of the line intensity along the slit of the spectrograph is similar to that of highly ionized species rather than to neutral species. Moreover the "transauroral" line [S I]458.93, proportional to [S I]772.50, should be detectable in our unpublished optical data, but is not. The detection of other C IV recombination lines is additional support to the correctness of our identification with C IV(8.01) (Moore 1970). The line has long ago been correctly assigned to C IV by Grandi (1976). The next odd-n line of the series is C IV(6-9), predicted at λ368.98, an unidentified line in KACE.

C IV(8–11)773.60 is relatively strong and the next odd members of C IV(8-n) coincides with unidentified optical lines noted by Aller et al. (1955) and KACE, e.g., λ586.5, perhaps 509.3, 468.0. Members of series C IV(9-n) and, quite probably, C IV(10-n) are detected, in the far-red, e.g., at λ720.7, 674.7, 870.7, 736.4. Some others should be significant contributors to blends (Paper IV). The highest C IV level positively detected by

means of an un-blended line may be $n = 23$ (λ702.19). Notice that all quasi-hydrogenic C IV lines involving large principal quantum numbers should be systematically blended with – and therefore enhanced by – homolog O IV (and occasionally N IV) lines, although the O IV lines were not explicitly listed in Table 2.

C IV(7–9) is barely seen in the wing of He I 706.5, but the next members of series C IV(7-n) systematically appear as relatively strong unidentified optical lines in the list of KACE at λ547.1, 468.9, 422.9 (blend [FeV]), etc., perhaps up to λ335.9 ($n = 17$).

Along the same isoelectronic sequence, N V(7-8)761.8 is clearly detected in spite of atmospheric absorption. Other relatively free N V lines may include two members of series N V(10-n) at λ892.6, 744.0.

4.5.3. C III

The large strength of C III(5g–6h)819.7 suggests other lines from higher levels may be detectable. However the highest large-l one-electron C III terms compiled by Moore (1970) are 6h, 7g, $6f^1$, and $7f^3$ (the latter with a question mark). Extrapolation is performed graphically, comparing with the very similar case of Si III for which higher levels are available (Moore 1965). The energy differences between Si III and C III and the departure of C III energies from pure hydrogenic energies are all assumed to vanish steadily as n and l increase. Analogous procedures were used by Péquignot et al. (1993) for several nitrogen and oxygen ions.

Then C III(5g–7h) and C III(5g–8h) are predicted at λ513.12, a strong unidentified line in KACE, and λ412.88, left unidentified by Aller et al. (1955) and wrongly identified as [Fe III](4F) by KACE (Garstang 1957). Many weaker optical C III lines are predicted and indeed detected in our unpublished spectra (Paper V). For illustration, a dozen such lines can be found in the captions for Figs. 3, 4, and 6 of Paper II, ~2/3 of them being sufficiently strong and un-blended to be effectively seen. Notice λ513.12 was commonly detected in bright planetary nebulae at a time unidentified lines used to be listed by observers (e.g., Aller & Walker 1970). It is suggested this line may provide a new diagnostic for carbon-abundance determination in planetary nebulae (according to Paper II, the contribution of [Kr V]513.13 should be small).

4.5.4. C II

Line C II(4f–5g)990.3, upstream from the well known C II 426.7 in radiative cascades, is strong enough to imply other C II recombination lines should be detectable. Thus the next members of the series (Moore 1970) appear at λ646.20, a strong unidentified line in the table of KAF, and λ534.24, visible in Fig. 2 (line "f") of Paper II. Several multiplets corresponding to transitions between low-energy one-electron levels are strong (e.g., λ723.1, 657.8).

The dielectronic-line spectrum of C II is rich. Note the core of the doublet line λ879.4 (line "d" in Fig. 15 of Paper II) is distinctly broader than the core of isolated lines (e.g., lines "a" or "f" in Fig. 15), although no blend was identified and the nearby strong He II cannot induce this effect. In fact He II itself is slightly broadened by a blend with the second component of the C II doublet and some other lines. Moreover C II 879.4 shows an extended blue wing (features "b"+"c"), which is essentially unidentified (the hardly significant weakest part "b" of the wing is very tentatively attributed to [P I], but no compelling spectroscopic confirmation is yet available, and feature "c" is not identified). A red wing would be hidden by He II. Line C II 879.4 is peculiar in that it is the only identified example in our spectra of a reasonably clear and strong dielectronic line arising *directly* from an autoionizing upper level (Moore 1970). The peculiar profile of this line is, we suggest, the spectroscopic signature of the very large natural width inherent to a strongly autoionizing level.

Multiplet C II(14) is a strong dielectronic quartet, displayed in Fig. 9 of Paper II. As noted by Grandi (1976), the presence of quartet lines is at first view quite surprising since recombination to C^+ should proceed almost exclusively from the ground state of C^{2+}, that is from a singlet term, and intercombination transitions are typically 10^4 times less frequent than normal dipole transitions. The explanation lies in the fact autoionizing transitions may indeed be 10^4 times faster than usual bound-bound transitions, so that intercombination transitions involving autoionizing levels may have transition rates comparable to dipole transitions. In favourable conditions, autoionizing quartet terms can build up a substancial population and then radiatively decay to bound terms (e.g., Nussbaumer & Storey 1984). The observed strength of the multiplet implies that dielectronic recombination to quartets is very effective and should be included in the total recombination rate coefficient of C II and other ions (Badnell 1988).

The highest one-electron terms tabulated by Moore (1970) are 7h, 8g, and 7f. Compared to C III, the extrapolation to higher levels of C II is easier in that only doublets need be considered and the departure from hydrogenic energies is weaker. Thus the uncertainty on the predicted wavelengths should not exceed the observational uncertainty. Many predicted C II lines are then found to nicely coincide with previously unidentified weak lines. Although blends are quite frequent, isolated members of all series corresponding to lower levels 5g, 5f, and 5d are probably detected (λ931.9, 757.4, 814.1, 751.0, 710.2, 887.4, 688.1). The fact no predicted C II line of any significance is absent from Table 2 indirectly confirms the reality of most lines left unidentified, however weak they may be. In the case of C II, extrapolation of levels is not expected to help identifying strong lines in existing optical tabulations, since strong recombination lines involve a few relatively low levels already tabulated by Moore (1970). Many weak lines are expected.

4.5.5. Neon

Levels $n = 6$ and 7 are unknown for Ne^{3+}. Transitions 6h–7i and 6g–7h are rather conspicuous for C IV772.6, N IV770.3, 758.2, and O IV771.3, 767.7. Homolog lines of Ne IV may not

be detectable, due either to unfavorable wavelengths (blend, etc) or to splitting of the terms in several weak components. Alternatively they may correspond to lines left unidentified. In the latter case, since nitrogen and neon have roughly similar abundances, the Ne IV lines should be quite strong. Here we tentatively suggest to identify Ne IV(6h–7i) and Ne IV(6g–7h) to lines λ774.65 and λ771.95, respectively. The former could be quite noticeable among unidentified lines, were it not for the proximity of the very strong [Ar III]775.1. The quoted intensity may be somewhat small for Ne IV, but no other candidate is apparent at least within ±40 nm of the hydrogenic wavelength. The latter line on the other hand should be weaker and therefore less "unique". Due to the small silicon abundance, only a small fraction of the selected line can be Si IV(6g-7h). Besides the observed wavelength is a poor match to that of Si IV.

Insufficient description of atomic energy levels is, we think, the main reason why no neon line could be identified, whereas a few magnesium and silicon lines and tens of nitrogen and oxygen lines were.

4.6. New forbidden lines and new elements

Longward of λ654.0 nm, Aller & Minkowski (1946) and KAF listed 15 and 19 forbidden lines respectively. About 10 more forbidden lines were registered in the range λ860.0–1040.0 (e.g., KACE). A total of 136 forbidden lines are listed in Table 2, out of which about 60% can be considered as genuinely detected at least after de-blending.

4.6.1. Heavy elements

Heavy elements were fully discussed in Paper II, in connection with optical spectra. The far-red range harbours lines of [Kr III], [Kr V], [Xe III], [Xe IV], [Se III], [Br III], [Br IV], [Sr IV], [Pb II]. Following Paper II, more lines are listed in Table 2 but cannot yet be taken as conclusive evidence for the presence of other heavy ions/elements (Cs, Te, Y, I, etc.) because of blends, weakness of the lines, wavelength misfit, etc.

A number of far-red lines seems to be best explained as due to iron-peak elements.

4.6.2. Iron

All iron ions present in NGC 7027 and emitting significant lines in the far-red were found.

Detection of [Fe II] (Johansson 1978) in NGC 7027 was previously reported by Péquignot & Baluteau (1988). Far-red [Fe II] lines are often strong in supernova remnants (e.g., Dennefeld 1982). Here a dozen [Fe II] lines from multiplets 1F, 13F, 14F, and possibly 43F are recorded. Good accuracy is achieved for several intensities.

[Fe IV] lines are recorded, particularly [Fe IV]699.7, which seems quite broad however and may be blended. There is a rather good case for the detection of multiplet ^{4}G-^{2}I (λ 674.0, 676.1, 673.4), which is not mentionned, e.g., in the compilation by Fuhr et al. (1988), who "selected all lines of at least moderate strength" (see also a comparison to the RR Tel spectrum by Ekberg & Edlén 1978). The multiplet was apparently neglected on the basis of the very long lifetime of its upper term. This "pre-Bowen" point of view is not tenable: at sufficiently low density, there is no reason why these lines should be weaker than any forbidden line, especially as their upper statistical weight is rather large and their branching ratio is unity. We suspect these lines will in fact be the strongest [Fe IV] lines in a majority of nebulae. Ekberg and Edlén correctly stated they are not seen in RR Tel owing to the high density.

In spite of unfavorable blends, [Fe V] is correctly detected at λ813.7 and possibly λ681.9.

Finally [Fe VII] is likely to contribute to λ660.1, also mentionned by KAF, although the intensity quoted in Table 2 is one order of magnitude below their detection limit.

4.6.3. Iron-peak elements

Nickel is represented by several [Ni II] lines, including a well known doublet, and [Ni III]789.0 (a second [Ni III] line is blended with P16), also detected in other types of nebulae (e.g., Osterbrock et al. 1990).

On the same isoelectronic sequence as [Ni III], the homolog line [Cu IV]694.9 is convincingly detected, the possible contribution of a C III(7–13) line being probably moderate. Again the next line, [Cu IV]759.1, is blended (Sugar & Musgrove 1990).

Although several [Mn II] lines are noted in Table 2, detection of this ion is not certain due to numerous blends. [Mn II]676.3 may appear as a very weak extension to a blend [Fe IV]+C III, from which it is in principle separated. In general [Mn II] lines seem to be systematically close to – but not coincident with – observed significant features. Accepting a ~0.2 nm shift of wavelengths would perhaps allow a larger intensity for this ion. However the accuracy of predicted wavelengths looks good (Sugar & Corliss 1985). In fact [Mn II]685.04 coincides with a strong line, λ684.96, left unidentified by KAF, which is almost certainly another manganese line, namely [Mn VI]685.21. In this case, the 0.25 nm difference in wavelength between observation and laboratory prediction is indirectly confirmed by optical [Mn VI] lines (unpublished material). Our wavelength determination improves on the value compiled by Martin et al. (1988).

Chromium is represented by several relatively strong lines from different ions (Martin et al. 1988; Sugar & Corliss 1985), including [Cr V](1F) 788.4, 758.1, perhaps 671.0, [Cr IV](2F) 691.5, 689.7, perhaps 674.7 (blended) and [Cr IV](1F) 739.1, and quite possibly [Cr II]800.0. The identification of chromium is virtually certain.

Other much more tentative detections are as follows.

Two ions of vanadium can emit in the far-red ([V IV]: Martin et al. 1988; energy levels of V III: Sugar & Corliss 1985). [V IV](1F) 940.1 may be part of a difficult blend, and [V IV]912.2 is blended. Line [V IV](2F) 785.7 is the best indication for this ion, although it is close to a stronger feature. Other members of the multiplet include [V IV]774.1, barely seen, and [V IV] 761.8, at unfavorable wavelength. Most lines of multi-

plets [V III](2F) and (1F) are blended with Paschen and other lines. One relatively free line is [V III]845.74, which may appear as an extension of one of the He I\6+7/ blends, 0.2 nm apart from an unidentified line.

Cobalt is represented by multiplet [Co III](^{4}F-^{4}P) (Fuhr et al. 1988), of which 3 components are a priori accessible. [Co III]685.36 is not seen between two quite strong lines separated by 0.6 nm, [Co III]696.14 may belong to a broad, essentially unidentified, feature centred at λ695.87, and [Co III]715.26 is close to a possible unidentified line λ715.17. The first unidentified line is in fact the most noticeable in our spectrum within 200 nm and the second may be quite strong too, but the underlying continuum is not accurately defined. Identification here is hampered by the absence of one of the strong lines. There is apparently no chance the predicted wavelenghs may be in error by as much as 0.2 nm (Hansen et al. 1984).

One [Ti III](2F)970.53 may be part of a blend. Other components of the multiplet belong to very unfavorable wavelengths around λ950 nm.

4.6.4. A new [S III] line

To our knowledge the quadrupolar electric line [S III] $^1D_2$–$^3P_0$ has never been observed before. From the data compiled by Kaufman & Sugar (1986), we deduce a wavelength λ = 882.965±0.03 nm for this transition. A then unidentified feature at λ883.0 nm, blended with He I\9/12, was already noticed in Paper I (see Fig. 2b and the end of Sect. 7.1 in that paper). A deeper spectrum provides a wavelength of 882.98±0.03 nm (Fig. 15 of Paper II), in excellent agreement with the calculated wavelength. According to Paper I, the He I line is weak compared to [S III]. A dielectronic O IV line is blended too, but should be rather weak (Paper IV).

4.6.5. [Cl III] wavelengths

Out of the four [Cl III](3F), only one, λ848.1 nm, is completely free from blend with Paschen lines, while λ843.4 nm is clearly visible in the wing of P18 (Fig. 2a of Paper I). Notice that the electric quadrupolar transition [Cl III] $^2D_{5/2}$–$^2P_{1/2}$ is predicted at λ854.80 nm from the data of Kaufman & Sugar (1986). Our observation confirms the energy levels given by these authors in that the line is barely detectable in the wing of P15 (Fig. 2a in Paper I), whereas it would be clearly separated using the older wavelength determination λ855.05 nm (e.g., Wiese et al. 1969; Mendoza 1983). Similarly, [Cl III]850.00, noted but not identified by KAF, is responsible for the broadening of P16 (λ850.2 nm) which would not be seen using the older wavelength (λ850.2).

4.7. Absorption features

The resonant multiplet K I(1) λ766.5, 769.9 is detected in absorption against the recombination continuum. Both lines are blueshifted by (27±10) km s^{-1} with respect to the emission lines, suggesting they may be produced in the expanding neutral shell surrounding the H$^+$ region. A purely interstellar origin is not excluded however.

Diffuse interstellar bands are not conspicuous in the far-red (e.g., Sanner et al. 1978) and are generally not evident in the present spectra. A noticeable exception is the relatively sharp and clear feature λ661.31.

5. Conclusion

Thanks to its brightness and to the richness of its spectrum, the planetary nebula NGC 7027 has been a reference object for more than half a century. The deep spectroscopy and thorough identification performed since the early 40's ended three decades ago. The current list of lines detected and identified in the optical is virtually the same as that of 1955. The last improvement in the optical dates back to 1963. At that time, pioneering spectrophotometry already provided an account of the bright lines in the far-red. Next works improved on intensities of known lines.

Evidently an effort similar to that of the 50's was called for, in order to raise the description of nebular spectra up to standards corresponding to present-day capabilities in astrophysical spectroscopy and atomic physics.

The far-red range was a priority since the available list of detected and identified far-red lines in NGC 7027 was scarcer than the list of optical lines available 50 years ago (except for hydrogen and helium lines, Paper I), whereas technology has made no difference between both wavelength ranges for more than a decade. Due to strong reddening, NGC 7027 was particularly appropriate to a far-red survey.

The present work aimed at establishing the far-red spectrum of NGC 7027. The result is a one-order-of-magnitude improvement in the rates of line detection and identification with respect to even the most recent studies.

At most wavelengths shortward of 900 nm, the limit of detection achieved after reddening correction approaches 10^{-6} of [O III], the strongest optical line. Owing to atmospheric absorption and declining sensitivity of the detector, detection is less effective at longer wavelengths.

Improvement upon the present data is still clearly possible, just on securing more spectra, particularly longward of 980 nm. Also the consequences of atmospheric absorption could perhaps be minimized, using higher spectral resolution and larger telescopes.

Concerning line identifications, a first quantitative assesment is being prepared (Paper IV) to justify and refine as much as possible the list of Table 2. It is foreseen that systematic spectral synthesis of the kind initiated by Péquignot et al. (1993) for nova spectra will become necessary in the future.

In the present form, the far-red spectrum already appears to be described in a more comprehensive manner than the optical one. The optical range is now clearly in need for a drastic update. The strong optical lines left unidentified in available surveys appear to essentially belong to two categories: (1) forbidden lines from heavy elements (Paper II) and (2) permitted lines from

relatively large nl terms of common elements (preliminary indications are provided in Sect. 4.5). However many more weak lines are to be expected. Analysis of deep optical spectra is in progress (Paper V: see captions to figures of Paper II) and should eventually result in a new homogeneous template spectrum for planetary nebulae and related objects.

Experimental and theoretical efforts to determine atomic energy levels, including the large-nl levels of the most common elements, are needed and possible to raise this branch of atomic physics to the standards of nebular spectroscopy. For example, theoretical atomic models could be developped and their results compared to nebular spectra, in much the same way forbidden lines were used in the past to check and improve experimental data. The lack of basic atomic data is pointed out as a major limitation to future progress in the field of nebulae.

References

Aller L.H., Bowen I.S., Minkowski R., 1955, ApJ 122, 62
Aller L.H., Bowen I.S., Wilson O.C., 1963, ApJ 138, 1013
Aller L.H., Keyes C.D., 1988, Proc. Natl. Acad. Sci. USA 85, 2417
Aller L.H., Minkowski R., 1946, PASP 58, 258
Aller L.H., Walker M., 1970, ApJ 161, 917
Atherton P.D., Hicks T.R., Reay N.K., et al., 1979, ApJ 232, 786
Badnell N.R.,1988, J. Phys. B 21, 749
Condal A., Fahlman G.G., Walker G.A.H., Glaspey J.W., 1981, PASP 93, 191
Danziger I.J., Goad L.E., 1973, Ap Letters 14, 115
Dennefeld M., 1982, A&A 112, 215
Dinerstein H.L., 1980, ApJ 237, 486
Butler S.E., Dalgarno A., 1980, A&A 85, 144
Ekberg J.O., Edlén, B., 1978, PS 18, 107
Eriksson K.B.S., 1978, ApJ 222, 398
Fuhr J.R., Martin G.A., Wiese W.L., 1988, J. Phys. Chem. Ref. Data 17 Suppl. No.4
Garstang R.H., 1957, MNRAS 117, 393
Grandi S.A., 1976, ApJ 206, 658
Hansen J.E., Raassen A.J.J., Uylings P.H.M., 1984, ApJ 277, 435
Howarth I.D., 1983, MNRAS 203, 301
Hummer D.G., Storey P.J., 1987, MNRAS 224, 801
Johansson S., 1978, PS 15, 183
Kaler J.B., Aller L.H., Czyzak S.J., Epps H.W., 1976, ApJS 31,163 (KACE)
Kaufman V., Martin G.A., 1991, J. Phys. Chem. Ref. Data 20, 83
Kaufman V., Sugar J., 1986, J. Phys. Chem. Ref. Data 15, 321
Keyes C.D., Aller L.H., Feibelman W.A., 1990, PASP 102, 59 (KAF)
Lemaitre G., Kohler D., Lacroix D., et al., 1990, A&A 228, 546
Martin G.A., Fuhr J.R., Wiese W.L., 1988, J. Phys. Chem. Ref. Data 17, Suppl. No.3
Mendoza C., 1983, in: Flower D.R. (ed.) IAU Symp. No. 103, Planetary nebulae. Reidel, Dordrecht, p. 143
Middlemass D., 1990, MNRAS 244, 294
Miller J.S., Mathews W.G., 1972, ApJ 172, 593
Moore C.E., 1965, Selected Tables of Atomic Spectra NSRDS-NBS 3, Sect. 1
Moore C.E., 1970, Selected Tables of Atomic Spectra NSRDS-NBS 3, Sect. 3
Moore C.E., 1971, Selected Tables of Atomic Spectra NSRDS-NBS 3, Sect. 4
Moore C.E., 1975, Selected Tables of Atomic Spectra NSRDS-NBS 3, Sect. 5
Moore C.E., 1976, Selected Tables of Atomic Spectra NSRDS-NBS 3, Sect. 7
Moore C.E., 1979, Selected Tables of Atomic Spectra NSRDS-NBS 3, Sect. 8
Moore C.E., 1980, Selected Tables of Atomic Spectra NSRDS-NBS 3, Sect. 9
Moore C.E., 1983, Selected Tables of Atomic Spectra NSRDS-NBS 3, Sect. 10
Moore C.E., 1985, Selected Tables of Atomic Spectra NSRDS-NBS 3, Sect. 11
Nussbaumer H., Storey P.J., 1984, A&AS 56, 293
O'Dell C.R., 1963, ApJ 138, 1013
Oke J.B., Gunn J.E., 1983, ApJ 266, 713
Osterbrock D.E., Shaw R.A., Veilleux S., 1990, ApJ 352, 561
Péquignot D., Aldrovandi S.M.V., Stasińska G., 1978, A&A 63, 313
Péquignot D., Baluteau J.–P., 1988, A&A 206, 298 (Paper I)
Péquignot D., Baluteau J.–P., 1994, A&A 283, 593 (Paper II)
Péquignot D., Petitjean P., Boisson C., Krautter J., 1993, A&A 271, 219
Petterson S.-G., 1982, PS 26, 296
Robberto M., Clampin M., Ligori S., Paresce F., Staude H.J., 1993, A&A 280, 241
Rudy R.J., Erwin P., Rossano G.S., Puetter R.C., 1992, ApJ 384, 536
Sanner F., Snell R., Vanden Bout P., 1978, ApJ 226, 460
Schwartz R.D., Peimbert M., 1973, Ap Letters 13, 157
Scrimger J.N., Lowe R.P., Moorhead J.M., Wehlau W.H., 1978, PASP 90, 257
Seaton M.J., 1979a, MNRAS 187, 73P
Seaton M.J., 1979b, MNRAS 187, 785
Sugar J., Corliss C., 1985, J. Phys. Chem. Ref. Data 14, Suppl. No.2
Sugar J., Musgrove A., 1990, J. Phys. Chem. Ref. Data 19, 527
Treffers R.R., Fink U., Larson H.P., Gautier T.N., 1976, ApJ 209, 793
Walton N.A., Pottasch S.R., Reay N.K., Taylor A.R., 1988, A&A 200, L21
Wenaker I., 1990, PS 42, 667
Wiese W.L., Smith M.W., Miles B.M., 1969, Atomic Transition Probabilities, Vol. 2, NSRDS-NBS 22
Woodward C.E., Pipher J.L., Forrest W.J., Moneti A., Shure M.A., ApJ 385, 567